



HAL
open science

Advanced measurements with contact in heat transfer: principles, implementation and pitfalls

Bertrand Garnier, François Lanzetta, Séverine Gomès

► To cite this version:

Bertrand Garnier, François Lanzetta, Séverine Gomès. Advanced measurements with contact in heat transfer: principles, implementation and pitfalls. Metti 6 Advanced School: Thermal Measurements and Inverse Techniques 2015, Mar 2015, Porquerolles, France. hal-02894725

HAL Id: hal-02894725

<https://hal.science/hal-02894725>

Submitted on 26 Jul 2021

HAL is a multi-disciplinary open access archive for the deposit and dissemination of scientific research documents, whether they are published or not. The documents may come from teaching and research institutions in France or abroad, or from public or private research centers.

L'archive ouverte pluridisciplinaire **HAL**, est destinée au dépôt et à la diffusion de documents scientifiques de niveau recherche, publiés ou non, émanant des établissements d'enseignement et de recherche français ou étrangers, des laboratoires publics ou privés.



Distributed under a Creative Commons Attribution 4.0 International License

Lecture 2: Measurements with contact in heat transfer: principles, implementation and pitfalls

B Garnier¹, F Lanzetta², S Gomès³

¹ Laboratoire de Thermocinétique UMR CNRS6607, Univ. Nantes, France
E-mail: bertrand.garnier@univ-nantes.fr

² FEMTO-ST, UMR CNRS 6174, Département ENERGIE, Université de Franche-Comté, Belfort, France

E-mail: francois.lanzetta@univ-fcomte.fr

³ Centre de l'Énergétique et de Thermique de Lyon UMR CNRS 5008, Université de Lyon, Villeurbanne, France

E-mail: severine.Gomès@insa-lyon.fr

Abstract. The main objective of this lecture is to make the end users aware of the various physical phenomena and especially of the errors frequently met during temperature and heat flow measurement. The lecture is divided in two main parts dealing with thermal measurement at macroscale and micro and nanoscales respectively. In Part 1, phenomena which occur in thermometry with contact (thermoelectric effects, thermoresistance) will be presented. For thermometry with contact, the analysis of systematic errors related to the local disturbance of field temperature due to the introduction of sensors will be emphasized. Indeed intrusive effects due to sensors are usually ignored and can be reduced using know how as will be shown through analytical modeling. Otherwise, interests of using semi intrinsic thermocouples will be discussed. The specificities of temperature measurement in fluid flow will be detailed. Finally heat flow measurement using direct methods (gradient, enthalpic, electric dissipation ...) or inverse methods (heat flow sensors with network of thermocouples) will be reminded. Part 2 focuses on fundamentals of Scanning Thermal Microscopy (SThM) methods. After a description of the main Scanning Probe Microscopy-based techniques developed for thermal imaging with a nanoscale spatial resolution, the approaches currently used for calibrating the SThM probes are given. In many cases, the link of the nominal measured signal to the research parameter is not yet fully established due to the complexity of the micro-/nanoscale interaction between the probe and the sample. Special attention is given to this micro/nanoscale interaction that conditions the tip-sample interface temperature, which is critical for many applications

1. Introduction: General notions about temperature sensors

Mediums are in interaction with the environment, the interaction can be of several types: thermal, electrical, magnetic, liquid or vapor mass transfer, chemical reaction, corrosion ... The installation of sensor on or inside the mediums should not modify these interactions. The choice of the sensor is performed so that these interactions do not have an effect on the measurement and on the lifespan of the sensor. For example, a sensor on a surface can modify heat transfer by conduction, convection or radiation. Otherwise, the deposit of a liquid film or a coating modifies emissivity and therefore the radiative heat exchanges. The main consequence is that the temperature provided by the sensor can be very different from the one to measure. One important thing to keep in mind is that temperature measurement is accompanied by parasitic effects which must be well-known.

According to the type of interaction between sensor and medium, one can classify the methods of

measurement in three categories:

1. *Methods with direct contact sensor-medium*: in this type of method, the sensor tends to locally equilibrate itself with the medium. If there is perfect adiabaticity of the sensor with the environment, its temperature is equal to that of the medium. However, in thermometric devices, this adiabaticity is usually not perfect.
2. *Methods with contact without physical connection with the environment*: in some cases, the temperature readings is carried out using an optical mean therefore no physical connection exists between the sensor and the environment. In this category, we can found surface temperature measurement with deposited thermosensitive material such as liquid crystals or photoluminescent salts.
3. *Methods without contact*: in this method sensors are far from the medium. Despite there is still interactions between them, the sensor is no more in equilibrium with the medium. Such methods are essentially based on radiative heat transfer.

In this lecture, one will discuss temperature measurement with contact. A focusing on the main methods (thermoelectric, thermoresistance) will be performed. First of all temperature measurement using thermoelectric effects will be analyzed in various situations (temperature measurement in fluids, in semi transparent medium and in opaque medium). Then recent progress for thermal measurement at micro and nanoscales using Scanning Thermal Microscopy methods will be presented.

2. Thermometry with contact: thermoresistances, thermocouples

2.1. Phenomena and sensors for temperature measurement

2.1.1. Thermoresistances

2.1.1.1. Metallic probes

They are commonly called Resistance Temperature Detectors (RTD). The thermosensitive parameter in these sensors is the electrical resistance. This one changes according to empirical law such as:

$$R = R_0 [1 + \alpha (T - T_0) + \beta (T - T_0)^2].$$

Their respective sensitivities, α , are about 10^{-3} K^{-1} that is rather weak, but their accuracy is rather large and higher than that of the thermocouples (Table 2.1). In the specified temperature range, their stability is good. The resistor probes have an almost linear answer. A resistance measurement device or a power supply with a low voltage voltmeter has to be used inducing a current about a few mA through the thermoresistive probes. One has to take care about self-heating or Joule effect in order to limit temperature bias. For practical applications, the thermoresistive probes are composed of a metallic layer deposited on a flat electrical insulating substrate (epoxy resin, ceramic, mica...) or cylindrical (glass, pyrex...). The size and the shape of these thermoresistive probes make them useful for average temperature measurement. In addition, their time constant is much larger than that of thermocouples due to their insulating substrate. Therefore they will be used preferentially for temperature measurement in stationary mode.

Table 2.1. Characteristics of the main thermoresistive metallic probes

Metal	Sensitivity α (K^{-1})	Temperature range ($^{\circ}\text{C}$)
Platinum	$4 \cdot 10^{-3}$	-200 à +1000
nickel	$6 \cdot 10^{-3}$	-190 à +350*
Copper	$4 \cdot 10^{-3}$	-190 à +150**

* : 358°C =Curie point for Nickel (magnetic transformation)

** : risk of oxydation for copper

2.1.1.2. *Thermistors*

The thermistors which are probes with semiconducting material are much more sensitive than the metallic probes (sensitivity 10 times larger), but they are less stable and their calibration curve is strongly nonlinear: $R = R_0 \exp [B (1/T - 1/T_0)]$.

The thermistors are presented in several shapes: pearl, disc or rod. The pearls are made of semiconducting material dropped on two connecting wires. Their diameter is about 0.15 to 2.5mm. They can be coated with glass. The flat discs are of more important size (2 to 25 mm in diameter and 0.5 to 12 mm thick). The rods are metalized at their extremity for the contact with the connecting wires. Their time constant ranges from a few seconds to several tens of seconds and the temperature range for thermistors goes usually from -50°C to 500°C.

2.1.2. *Thermoelectric effects: theory and practice*

The thermocouple is the most widely electrical sensor in thermometry and it appears to be the simplest of electrical transducers. Thermocouples are inexpensive, small in size, rugged, and remarkably accurate when used with an understanding of their peculiarities. Accurate temperature measurements are typically important in many scientific fields for the control, the performance and the operation of many engineering processes. A simple thermocouple is a device which converts thermal energy to electric energy. Its operation is based upon the findings of Seebeck [1]. When two different metals *A* and *B* form a closed electric circuit and their junctions are kept at different temperatures T_1 and T_2 (Figure 2.1), a small electric current appears.

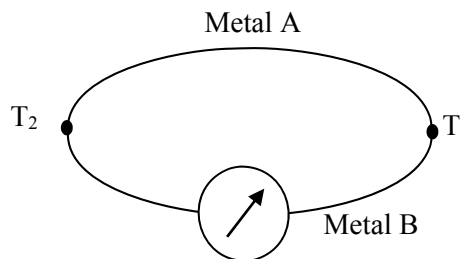


Figure 2.1. Thermocouple circuit.

The electromotive force, emf, produced under these conditions is called the Seebeck emf. The amount of electric energy produced is used to measure temperature. The electromotive force depends on materials used in the couple and the temperature difference $T_1 - T_2$. Seebeck effect is actually the combined result of two other phenomena, Peltier effect [2] and Thomson effect [3]. Peltier discovered that temperature gradients along conductors in a circuit generate an emf. Thomson observed the existence of an emf due to the contact of two dissimilar metals and related to the junction temperature. Thomson effect is normally much smaller in magnitude than the Peltier effect and can be minimized and disregarded with proper thermocouple design.

a) *Peltier effect*

A Peltier electromotive force $V_M - V_N$ is created at the junction of two different materials (wire or film) *A* and *B*, at the same temperature T , depending on the material and the temperature T (Figure 2.2):

$$V_M - V_N = \Pi_{AB}^T \tag{2.1}$$

Π_{AB} is the Peltier coefficient at temperature T .

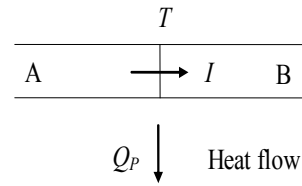
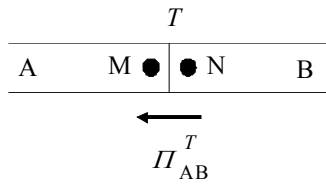


Figure 2.2. Peltier effect without current flow. **Figure 2.3.** Peltier effect with current flow.

When a current I flows through a thermocouple junction (Figure 2.3), heat, Q_p , is either absorbed or dissipated depending on the direction of current. This effect is independent of Joule heating.

$$dQ_p = (V_M - V_N)Idt = \Pi_{AB}^T Idt \quad (2.2)$$

Q_p is the heat quantity exchanged with the external environment to maintain the junction at the constant temperature T .

The phenomena are reversible, depending on the direction of the current flow and:

$$\Pi_{AB}^T = -\Pi_{BA}^T \quad (2.3)$$

b) *Volta's law*

In an isothermal circuit composed by different materials, the sum of the Peltier EMFs is nul (Figure 2.4) and:

$$\Pi_{AB} + \Pi_{BC} + \Pi_{CD} + \Pi_{DA} = 0 \quad (2.4)$$

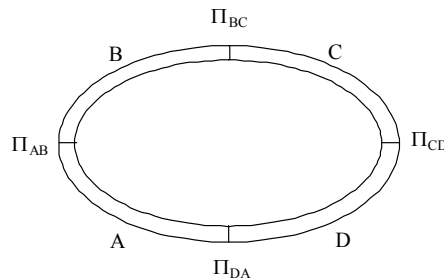


Figure 2.4. Volta's law with four materials.

c) *Thomson effect*

Thomson EMF's corresponds to the tension $e_A(T_1, T_2)$ between two points M and N of the same conductor, submitted to a temperature gradient, depending only on the nature of the conductor (Figure 2.5):

$$e_A(T_1, T_2) = \int_{T_1}^{T_2} \tau_A dT \quad (2.5)$$

Where τ_A is the Thomson coefficient of the material A.

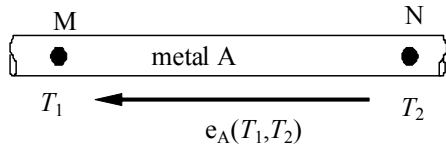


Figure 2.5. Thomson effect without current flow.

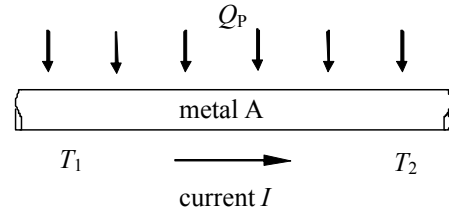


Figure 2.6. Thomson effect with current flow.

When a current I flows through a conductor within a thermal gradient ($T_1 - T_2$), heat Q_T is either absorbed or dissipated (Figure 2.6):

$$dQ_T = e_A(T_1, T_2) I dt = \int_{T_1}^{T_2} \tau_A dT I dt \quad (2.6)$$

d) *Seebeck effect*

When a circuit is formed by a junction of two different metals A and B and the junctions are held at two different temperatures, T_1 and T_2 , a current I flows in the circuit caused by the difference in temperature between the two junctions (Figure 2.7).

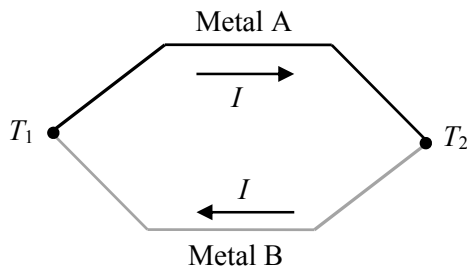


Figure 2.7. Seebeck effect.

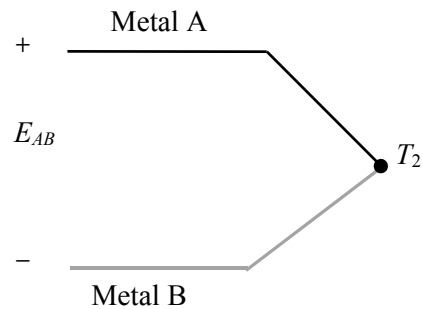


Figure 2.8. Seebeck Voltage.

The sum of the different Peltier and Thomson EMF for the circuit corresponds to the Seebeck EMF:

$$E_{AB}(T_2, T_1) = \Pi_{AB}^{T_1} + \Pi_{BA}^{T_2} + \int_{T_1}^{T_2} \tau_B dT + \int_{T_2}^{T_1} \tau_A dT \quad (2.7)$$

$$E_{AB}(T_2, T_1) = \Pi_{AB}^{T_1} - \Pi_{AB}^{T_2} + \int_{T_2}^{T_1} (\tau_A - \tau_B) dT$$

Then, the Seebeck EMF becomes:

$$E_{AB}(T_1, T_2) = \sigma_{AB}(T_1 - T_2) \quad (2.8)$$

σ_{AB} is the Seebeck coefficient for the A and B metals of the couple ($\mu\text{V}^\circ\text{C}^{-1}$ or μVK^{-1}). This coefficient corresponds to a constant of proportionality between the Seebeck voltage and the temperature difference.

If the circuit is open at the center of the circuit (Figure 2.8), the net open voltage is a function of the junction temperature and the composition of the two metals.

The thermoelectric power, or sensitivity, of a thermocouple is given by Table 2.2:

$$\sigma_{AB} = \frac{dE_{AB}}{dT} \tag{2.9}$$

Table 2.2. Seebeck coefficients of various thermocouple materials relative to platinum at 0°C [4]

Material	Seebeck coefficient ($\mu\text{V}^\circ\text{C}^{-1}$)	Material	Seebeck coefficient ($\mu\text{V}^\circ\text{C}^{-1}$)
Bismuth	-72	Silver	6.5
Constantan	-35	Copper	6.5
Alumel	-17.3	Gold	6.5
Nickel	-15	Tungsten	7.5
Potassium	-9	Cadmium	7.5
Sodium	-2	Iron	18.5
Platinum	0	Chromel	21.7
Mercury	0.6	Nichrome	25
Carbon	3	Antimony	47
Aluminium	3.5	Germanium	300
Lead	4	Silicium	440
Tantalum	4.5	Tellurium	500
Rhodium	6	Selenium	900

Thermocouples are made by the association of dissimilar materials producing the biggest possible Seebeck. In industrial processes, the common thermocouples are presented in Table 2.3.

2.2. Temperature measurement in fluids

2.2.1. Mathematical modelling

Transient phenomena appear in many industrial processes and many researchers and engineers have been paying attention to the measurement of temperature fluctuations in turbulent reacting flows, compressible flows, boiling, cryogenic apparatus, fire environments, under the condition of simultaneous periodical variations of velocity, flow density, viscosity and thermal conduction in gas [7-14].

Table 2.3. Thermocouple Types [5]

Type	Metal A (+)	Metal B (-)	Temperature range	Seebeck coefficient α ($\mu\text{V}/^\circ\text{C}$) at $T^\circ\text{C}$	Standard error	Minimal error	Comments
B	Platinum-30% Rhodium	Platinum-6% Platinum	0°C to 1820°C	$5.96 \mu\text{V}$ at 600°C	0.5%	0.25%	Idem R type (glass industry)
E	Nickel 10% Chromium	Copper-Nickel alloy (Constantan)	-270°C to 1000°C	$58.67 \mu\text{V}$ at 0°C	1.7% to 0.5%	1% to 0.4%	Interesting sensitivity
J	Iron	Copper-Nickel alloy (Constantan)	-210°C to 1200°C	$50.38 \mu\text{V}$ at 0°C	2.2% to 0.75%	1.1% to 0.4%	For atmosphere reduced (plastic industry)
K	Nickel-Chromium alloy (Chromel)	Nickel-luminium alloy (Alumel)	-270°C to 1372°C	$39.45 \mu\text{V}$ at 0°C	2.2% to 0.75%	1.1% to 0.2%	The most widely used because of its wide temperature range, supports an oxidizing atmosphere
N	Nickel-Chromium-Silicium alloy (Nicrosil)	Nickel-Silicium alloy (Nisil)	-270°C to 1300°C	$25.93 \mu\text{V}$ at 0°C	2.2% to 0.75%	1.1% to 0.4%	New combination very stable
R	Platinum-13% Rhodium	Platinum	-50°C to 1768°C	$11.36 \mu\text{V}$ at 600°C	1.5% to 0.25%	0.6% to 0.1%	High temperature applications, resists oxidation
S	Platinum-10% Rhodium	Platinum	-50°C to 1768°C	$10.21 \mu\text{V}$ at 600°C	1.5% to 0.25%	0.6% to 0.1%	Idem R type
T	Copper	Copper-Nickel alloy (Constantan)	-270°C to 400°C	$38.75 \mu\text{V}$ at 0°C	1% to 0.75%	0.5% to 0.4%	Cryogenic applications
W	Tungsten	Tungsten-26% Rhenium	$+20^\circ\text{C}$ to $+2300^\circ\text{C}$				Sensitive to oxidizing atmospheres, linear response and good performance in high temperature
W3	Tungsten-3% Rhenium	Tungsten-25% Rhenium	$+20^\circ\text{C}$ to $+2000^\circ\text{C}$				Idem W type
W5	Tungsten-5% Rhenium	Tungsten-26% Rhenium	$+20^\circ\text{C}$ to $+2300^\circ\text{C}$				Idem W type

There has been considerable progress in recent years in transient thermometry techniques. Some of these techniques are applicable for both solid material characterization while others are suitable only for fluids thermometry. This chapter deals only with temperature thermocouples measurements in fluids (gases and liquids). Many concepts involved in the temperature measurements in fluids are common to both types and they are discussed here. The techniques for temperature measurement in a fluid consists in inserting a thermocouple, allowing it to come to thermal equilibrium and measuring the generated electrical signal. When a thermocouple is submitted to a rapid temperature change, it will take some time to respond. If the sensor response time is slow in comparison with the rate of change of the

measured temperature, then the thermocouple will not be able to faithfully represent the dynamic response of the temperature fluctuations. Then, the problem is to measure the true temperature of the fluid because a thermocouple gives its own temperature only. The temperature differences between the fluid and the sensor are also influenced by thermal transport processes taking place between the fluid to be measured, the temperature sensor, the environment and the location of the thermocouple. Consequently, the measured temperature values must be corrected. Whereas in steady conditions only the contributions of the conductive, convective and radiative heat exchanges with the external medium occur, unsteady behavior introduces another parameter which becomes predominant : the junction thermal lag which is strongly related to its heat capacity and thermal conductivity. The corrections generally decrease with the thermocouple diameters, and both temporal and spatial resolutions are improved. However, while spatial resolution is fairly directly connected with the thermocouple dimensions, the temporal resolution doesn't only depend on the dimensions and the thermocouple physical characteristics, but also on the rather complex heat balance of the whole thermocouple. To obtain the dynamic characteristics of any temperature probe, we analyze its response to an excitation step from which the corresponding first time constant τ can be defined as :

$$\tau = \frac{\rho c V}{h A} \tag{2.10}$$

τ is the time constant, ρ the density, c the specific heat, V the volume of the thermocouple and A the area of the fluid film surrounding the thermocouple while h is the heat transfer coefficient.

The goal of this work consists in calculating or measuring time constants of thermocouples and comparing their behavior according to different dynamical external heating like convective, radiative and pseudo-conductive excitations.

An accurate calibration method is an essential element of any quantitative thermometry technique and the goal of any measurement is to correctly evaluate the difference between the "true" temperature and the sensor temperature. Figure 2.9. shows the energy balance performed at the butt-welded junction of a thermocouple for a junction element dx resulting from the thermal balance between the rate of heat stored by the junction $d\dot{Q}_{th}$ and heat transfer caused by:

- convection in the boundary layer around the thermocouple $d\dot{Q}_{cv}$
- conduction along the wires $d\dot{Q}_{cd}$
- radiation between the wires and the external medium $d\dot{Q}_{rad}$
- contribution of another source of heat power (a laser source in this example) $d\dot{Q}_{ext}$.

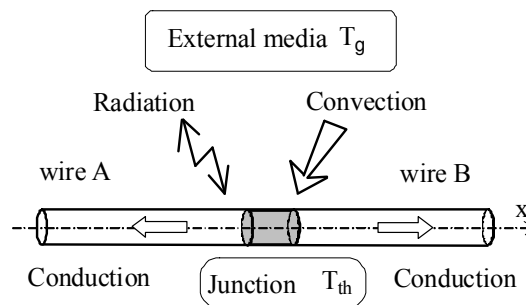


Figure 2.9. Heat balance for the probe

During a transient period, because of its thermal capacity, the thermocouple temperature will lag behind any gas temperature variation. This leads to an error from which a thermocouple time constant can be defined. The general heat balance for a junction of length dx is expressed as :

$$d\dot{Q}_{th} = d\dot{Q}_{cv} + d\dot{Q}_{cd} + d\dot{Q}_{rad} + d\dot{Q}_{ext} \quad (2.11)$$

The thermoelectric junction stores the heat by unit time $d\dot{Q}_{th}$:

$$d\dot{Q}_{th} = \rho_{th} c_{th} \frac{\pi d^2}{4} \frac{\partial T_{th}}{\partial t} dx \quad (2.12)$$

where ρ_{th} , c_{th} and T_{th} are the density, the specific heat and the temperature of the junction respectively. The junction is approximated by a cylinder whose diameter equals the wire diameter d . This does not exactly fit reality but remains currently used in numerical calculations [15-21]. Moreover, if the wires are uniformly curved, the observation near the junction confirms the previous assumption (Figures 3.20 and 3.21). The Newton's law of cooling is:

$$d\dot{Q}_{cv} = \pi dx Nu \lambda_g (T_g - T_{th}) \quad (2.13)$$

where λ_g and T_g are the thermal conductivity and the static temperature of the gas. The difficulty is to obtain an accurate relation between the Nusselt number Nu and the flow characteristics around the junction assumed as a cylinder [17, 22-25].

Indeed, such a thermocouple is surrounded by both a thermal and aerodynamic gradient which acts as a thermal resistance that is estimated from empiric approaches. A purely convective heat transfer coefficient h is generally deduced from correlations about the Nusselt number that is generally expressed as a combination of other dimensionless numbers, such as Eckert, Reynolds, Prandtl or Grashof numbers. However, if many cases have been investigated, the example of thin cylinders cooling process is still an open question. Table 2.4 gives a list of the main Nusselt correlations in this particular case.

Conduction heat transfer $d\dot{Q}_{cd}$ that occurs along the wires to the thermocouple supports has the following general expression:

$$d\dot{Q}_{cd} = \lambda_{th} \frac{\pi d^2}{4} \frac{\partial^2 T_{th}}{\partial x^2} dx \quad (2.14)$$

However, different studies and experiments have shown that conduction dissipation effects along cylindrical wires can be neglected when the aspect ratio between the length and the diameter is large enough [6, 26-32]. Indeed, practical cases of anemometry and thermometry have led to fix a condition such:

$$L/d > 100 \quad (2.15)$$

Hence, the temperature gradient can be considered null in the axial direction of the thermocouple wire. The thermocouple is placed in an enclosure at temperature T_w . The enclosure dimensions are assumed to be large with respect to the probe dimensions. Then, the influence of the radiative heat transfer can be expressed by the simplified form:

Table 2.4 Heat transfer laws – These laws describe the heat transfer from a cylinder of infinite length. The film temperature T_{film} is defined as the mean value between the fluid temperature T_f and the thermocouple temperature T_{th} [16-18, 20-25, 29-33]

Author	Temperature for λ , ρ and μ	Correlation	Reynold's number domain
Andrews	T_f	$Nu = 0.34 + 0.65 Re^{0.45}$	$0.015 < Re < 0.20$
Bradley and Mathews	T_f	$Nu = 0.435 Pr^{0.25} + 0.53 Pr^{0.33} Re^{0.52}$	$0.006 < Re < 0.05$ $0.7 < Pr < 1$
Churchill et Brier	T_f	$Nu = 0.535 Re^{0.50} (T_f / T_{th})^{0.12}$	$300 < Re < 2300$
Collis and Williams	T_{film}	$Nu = (0.24 + 0.56 Re^{0.45}) (T_{film} / T_{gaz})^{0.17}$	$0.02 < Re < 44$
Collis an Williams	T_{film}	$Nu = (0.48 Re^{0.45}) (T_{film} / T_{gaz})^{0.17}$	$44 < Re < 140$
Davies and Fisher	T_f	$Nu = (2.6/\gamma\pi) Re^{0.33}$	$0.01 < Re < 50$
Eckert and Soehngen	/	$Nu = 0.43 + 0.48 Re^{0.5}$	$1 < Re < 4000$
Glawe and Johnson	T_f	$Nu = 0.428 Re^{0.50}$	$400 < Re < 3000$
King	T_{film}	$Nu = 0.318 + 0.69 Re^{0.5}$	$0.55 < Re < 55$
Kramers	T_{film}	$Nu = 0.42 Pr^{0.2} + 0.57 Pr^{0.33} Re^{0.5}$	$0.01 < Re < 10000$ $0.7 < Pr < 1000$
McAdams	T_{film} and T_f for ρ	$Nu = 0.32 + 0.43 Re^{0.52}$	$40 < Re < 4000$
Olivari and Carbonaro	T_{film}	$Nu = 0.34 + 0.65 Re^{0.45}$	$0.015 < Re < 20$ $L / d > 40$
Parnas	T_f	$Nu = 0.823 Re^{0.5} (T_{th} / T_f)^{0.085}$	$10 < Re < 60$
Richardson	/	$Nu = 0.3737 + 0.37 Re^{0.5} + 0.056 Re^{0.66}$	$1 < Re < 10^5$
Scadron and Warshawski	T_f	$Nu = 0.431 Re^{0.50}$	$250 < Re < 3000$
Van den Hegge Zijnen	T_{film}	$Nu = 0.38 Pr^{0.2} + (0.56 Re^{0.5} + 0.01 Re) Pr^{0.33}$	$0.01 < Re < 10^4$

$$d\dot{Q}_{rad} = -\sigma \varepsilon(T_{th}) (T_{th}^4 - T_w^4) dS_{ray} \quad (2.16)$$

σ is the Stefan Boltzmann constant and $\varepsilon(T_{th})$ the emissivity of the wire at the temperature T_{th} . The exchange surface of the radiative heat transfer $dS_{rad} = \pi d dx$ nearly equals the surface exposed to the convective heat flux. This supposes that the radiative heat transfer between the sensor and the walls is greater than between the gas and the sensor. Here, the assumption is that the gas is transparent, however it is not satisfied in several practical applications like temperature measurements in flames.

In section 2.2.1.b we will consider a radiative calibration so that the thermocouple junction is submitted to an external heat contribution $d\dot{Q}_{ext}$ produced by a laser beam [27].

$$d\dot{Q}_{ext} = \sqrt{\frac{2}{\pi}} \frac{(1-\bar{R})}{a} P_L \operatorname{erf}\left[\frac{d}{a\sqrt{2}}\right] \exp\left[-2\frac{x^2}{a^2}\right] dx \quad (2.17)$$

P_L is the laser beam power, \bar{R} the mean reflection coefficient of the thermocouple junction surface, d the diameter of the junction and a the laser beam radius (this value corresponds to the diameter for which one has 99 % of the power of the laser beam).

The total heat balance of the thermocouple may be written as follows

$$\begin{aligned} \rho_{th} c_{th} \frac{\pi d^2}{4} \frac{\partial T_{th}}{\partial t} = Nu \lambda_g \pi (T_g - T_{th}) + \lambda_{th} \frac{\pi d^2}{4} \frac{\partial^2 T_{th}}{\partial x^2} \\ - \sigma \varepsilon(T_{th}) (T_{th}^4 - T_w^4) \pi d + \sqrt{\frac{2}{\pi}} \frac{(1-\bar{R})}{a} P_L \operatorname{erf}\left[\frac{d}{a\sqrt{2}}\right] \exp\left[-2\frac{x^2}{a^2}\right] \end{aligned} \quad (2.18)$$

The expression of the gas temperature T_g is deduced from equation (2.18):

$$T_g = T_{th} + \tau_{cv} \left[\begin{aligned} & \frac{\partial T_{th}}{\partial t} - \frac{\lambda_{th}}{\rho_{th} c_{th}} \frac{\partial^2 T_{th}}{\partial x^2} + \frac{4 \sigma \varepsilon(T_{th})}{\rho_{th} c_{th} d} (T_{th}^4 - T_w^4) \\ & - \frac{4}{\rho_{th} c_{th} d^2} \sqrt{\frac{2}{\pi}} \frac{(1-\bar{R})}{a} P_L \operatorname{erf}\left[\frac{d}{a\sqrt{2}}\right] \exp\left[-2\frac{x^2}{a^2}\right] \end{aligned} \right] \quad (2.19)$$

Equation 2.19 represents a general expression of the thermocouple dynamic behavior including each of the heat transfer modes. In this expression, the time constant τ_{cv} of the thermocouple junction is defined by:

$$\tau_{cv} = \frac{\rho_{th} c_{th} d^2}{4 Nu \lambda_g} = \frac{\rho_{th} c_{th} d}{4 h} \quad (2.20)$$

If the radiation, the conduction and the external heat supply are neglected, the gas temperature simplifies to:

$$T_g = T_{th} + \tau_{cv} \frac{\partial T_{th}}{\partial t} \quad (2.21)$$

The time-response of a temperature sensor is then characterized by a simple first order equation. This is a common but erroneous way. For a step change in temperature, equation (2.21) reduces to:

$$\frac{T_g - T_{th}}{T_g - T_i} = \exp\left[-\frac{t}{\tau_{cv}}\right] \quad (2.22)$$

where T_i is the initial temperature.

Conventionally, the time constant τ_{cv} is defined as the duration required for the sensor to exhibit a 63%, ($= 1 - e^{-1}$) change from an external temperature step, in the case of a single-order equation. Actually, the fact that different kinds of heat transfers are involved should lead to a global time-constant in which the different phenomena contributions are included [16, 29]. As a consequence, the ability of a thermocouple to follow any modification of its thermal equilibrium is resulting from a multi-ordered time response where the most accessible experimental parameter remains the global time constant. The multi-ordered temperature response of a thermocouple can be represented by the general relation:

$$\frac{T_g - T_{th}}{T_g - T_i} = K_1 \exp\left[-\frac{t}{\tau_1}\right] - K_2 \exp\left[-\frac{t}{\tau_2}\right] - \dots - K_n \exp\left[-\frac{t}{\tau_n}\right] \quad (2.23)$$

T_i is the initial temperature, T_g is the fluid temperature. The value of the constants K_1, K_2, \dots, K_n as well as the time constants $\tau_1, \tau_2, \dots, \tau_n$, depend on the heat flow pattern between the thermocouple and the surrounding fluid.

If experiments have shown that most configurations involve nearly first-order behaviors, the measured time-constant does not allow to isolate each of the different contribution modes.

Therefore, the remaining problem of experiments is to relate this global time-constant to the different implied heat transfer modes. Then, our contribution in this section will be to show the influence of the heat transfer condition on the measured time constant value through three different methods of dynamic calibration.

Classical testing of thermocouples often involves plunging them into a water or oil bath and for providing some information only about the response of the thermocouple under those particular conditions. It does not provide information about the sensor response under process operating conditions where the sensor is used. In order to improve thermocouple transient measurements, a better understanding of the dynamic characteristics of the sensor capability is necessary.

2.2.2. Dynamic calibration

The calibration methods consist of a series of heating and cooling histories performed by submitting the thermocouple to different excitation modes. Then, the resulting exponential rise and decay times of the thermocouple signals allow to estimate the time constant τ . The thermocouple signal is amplified with a low-noise amplifier having a -3 dB bandwidth of 25 kHz (Gain = 1000). The output voltage is finally recorded by a digital oscilloscope.

a) Convective calibration

Figure 2.10. illustrates the convective experimental device. The thermocouple junction is exposed continuously to a constant cold air-stream at constant temperature T_{MIN} . A second hot air flow excites periodically the thermocouple and creates a temperature fluctuation of frequency f [33].

The response of a thermocouple submitted to successive steps of heating or cooling is close to a classical exponential first order response from which the time constant can be determined (Figure 2.11.). It can be deduced from the measurement of four temperatures: T_{MAX} , T_{MIN} , $T_{th\ max}$ and $T_{th\ min}$.

For the heating period t_h , we define the temperature differences δ_{1h} and δ_{2h} :

$$\delta_{1h} = T_{MAX} - T_{th\ min} \quad \text{and} \quad \delta_{2h} = T_{MAX} - T_{th\ max} \quad (2.24), (2.25)$$

For the cooling period t_c , the temperature differences δ_{1c} and δ_{2c} by:

$$\delta_{1c} = T_{th\ max} - T_{MIN} \quad \text{and} \quad \delta_{2c} = T_{th\ min} - T_{MIN} \quad (2.26), (2.27)$$

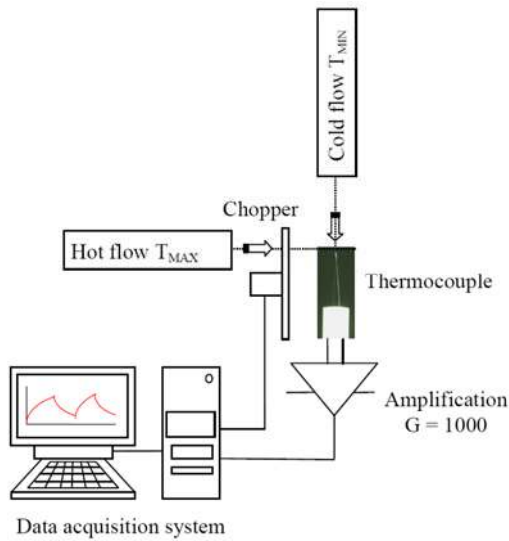


Figure 2.10. Convective characterization setup

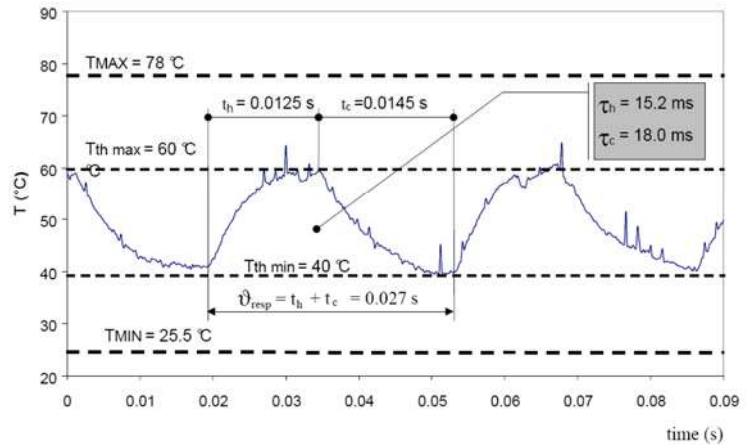


Figure 2.11. Convective characterization results

Then, the two convective time constants are defined while the thermocouple is heating (τ_h) and cooling (τ_c). If we consider a first order response of the sensor we obtain the expressions:

$$\tau_h = \frac{t_h}{\ln(\delta_{1h}/\delta_{2h})} \text{ and } \tau_c = \frac{t_c}{\ln(\delta_{1c}/\delta_{2c})} \quad (2.28), \quad (2.29)$$

Then the period of the thermocouple response is:

$$\mathcal{P}_{resp} = t_c + t_h \quad (2.30)$$

Figure 2.11 presents temperature histories for a 12.7 μm K type thermocouple. The excitation frequency is 37 Hz. The velocities of hot and cold air are both 13 $\text{m}\cdot\text{s}^{-1}$ at the outlet of the air flow tubes. In any case, the measured time constants are longer during the heating phase than during the cooling one. This phenomenon corresponds to a greater magnitude of the convection coefficient (h). Table 2.5 presents convective time constants for the different thermocouple diameters, resulting from heating periods only and for two air flow velocities (13 $\text{m}\cdot\text{s}^{-1}$ and 23 $\text{m}\cdot\text{s}^{-1}$) and for a 5 to 72 Hz explored frequency bandwidth.

Table 2.5 Convective time constant τ_{cv} (ms) and bandwidth Δf (Hz) versus junction diameters. The thermocouple mechanical resistance is not sufficient for the flows with 13 $\text{m}\cdot\text{s}^{-1}$ and 23 $\text{m}\cdot\text{s}^{-1}$ air velocities

Junction diameter d (μm)	Air velocity : 13 $\text{m}\cdot\text{s}^{-1}$		Air velocity : 23 $\text{m}\cdot\text{s}^{-1}$		
	τ_{cv} (ms)	Δf (Hz)	τ_{cv} (ms)	Δf (Hz)	
S	0.5	–	–	–	
	1.27	–	–	–	
	5	2.9	55	2.2	72
K	12.7	15.2	10.5	8.5	18.7
	25	20	8	17	9.4
	250	32	5	25	6.4

One can notice that time constants decrease when increasing the flow velocity because of a larger surface over volume ratio exposed to the flow. Finally, even if the repeatability is good, such a calibration method remains however quite difficult to perform because the fragility of the sensor increases when the wires dimension decreases and the fluid flow increases.

b) Radiative calibration

This calibration method is based on a radiative excitation produced by a continuous argon laser [34, 35]. A set of two spherical lenses allows to locate the beam waist on the junction and an optical chopper generates a periodic modulation of the continuous laser beam. In order to avoid parasitic turbulences around the junction, the sensor is placed in a transparent enclosure (Figure 2.12.).

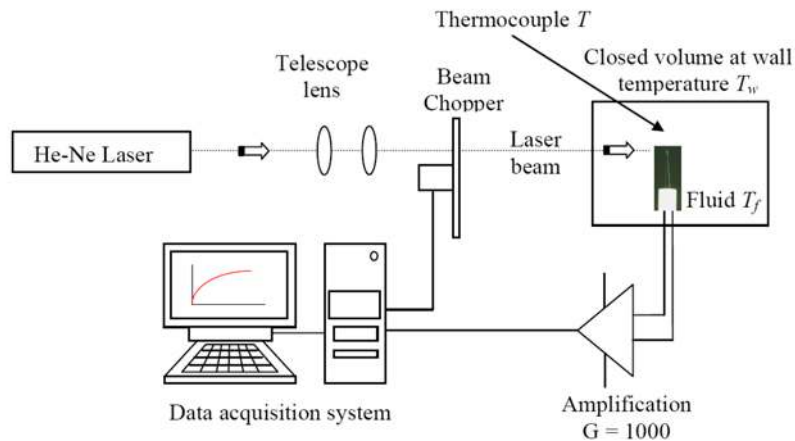


Figure 2.12. Radiative characterization setup

The signal obtained is close to a first order response which gives immediately the sensors dynamic performances. Time constants decreases as diameter and heat transfer (the laser power) increase (Figure 2.13.). This is consistent with the effect of an increasing value of the power density or a decreasing of the beam radius that both acts on the power to heated mass ratio. Table 2.6 presents the radiative time constant for all the thermocouple junction diameters and the explored frequency bandwidth is ranged from 5 to 2274 Hz.

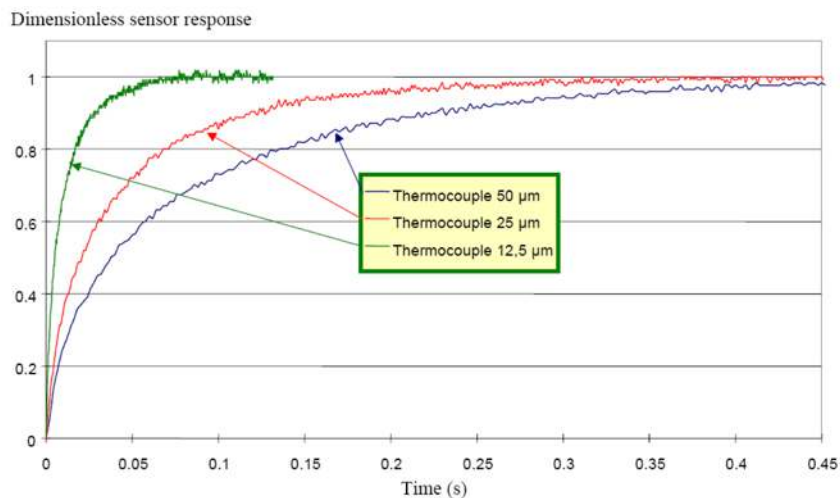


Figure 2.13.

Table 2.6 Radiative time constant τ_{rad} (ms) and bandwidth Δf (Hz) versus junction diameters

Junction diameter	Radiative time constant	Bandwidth
d (μm)	τ_{rad} (ms)	Δf (Hz)
S	0.5	2274
	1.27	884
	5	123
	12.7	19
K	25	5
	50	2.5

2.2.3. *Microthermocouple designs*

Different methods are used to design a thermocouple probe. It consists of a sensing element assembly, a protecting tube and terminations. Two dissimilar wires are joined at one end to form the measuring junction which can be a bare thermocouple element twisted and welded or butt welded. The protecting tube protects the sensing element assembly from the external atmosphere by a non ceramic insulation, a hard fired ceramic insulator or a sheeted compact ceramic insulator.

The thermocouple probe consists of two wires inserted in a ceramic double bore tube with length and external diameter depending on the experimentation. The wires are cut with a razor blade to produce a flat edge perpendicular to the axis. To realize the junction the thermocouple wires are connected to a bank of condensers (Figure 2.14.).

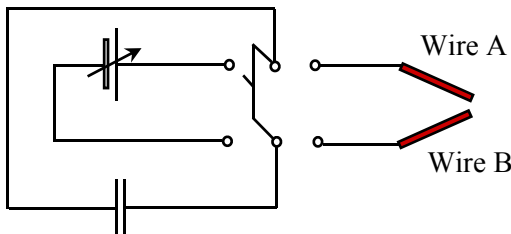


Figure 2.14. Thermocouple welding apparatus

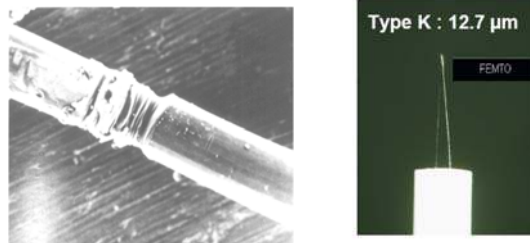


Figure 2.15. Thermocouple junction and probe

The two extremities are approached together in the same time and the beaded junctions are made by a sparking method. The energy release produced by the couple voltage-capacitance is sufficient to weld together the wires. One advantage of this technique is that the resulting junction diameter is not significantly greater than the wires one (Figure 2.15.). Except low mass and specific heat, another consequence is that the cross-sectional area of the wire itself can be used to calculate time constants. A drop of glue can be deposited at the tube extremity and pushed down around both wires to minimize the probe fragility.

2.3. Error introduced by the disturbance of the local temperature using thermocouples

2.3.1. Introduction

Whatever the selected measurement method, it is accompanied by parasitic effects which must be well-known. The resulting errors can be classified in two categories:

- the ones that are directly related to the thermometric phenomenon, they correspond to the inaccuracy on the measurement of thermometric quantities and to the parasitic effects attached to this phenomenon. It is not here the main topic, but they are not less important. We will quote simply for memory: singularities met in the laws of variation of electrical resistance due to structure modifications (allotropic transformations...), with chemical attacks... and for the thermoelectric circuits, the many parasitic effects such as e.m.f. induced, modifications of the thermoelectric force due to heterogeneities, modifications of structure, junctions nonspecific and not isotherms.
- the others, independently of the selected sensor are related to the fact that the interaction between thermometer, medium and environment causes a local disturbance of the temperature field therefore the local temperature is no more the one that exists before thermometric sensor settling.

In the following, we will present an error analysis and models to describe the local disturbance due to the presence of the sensors. These results come from various works performed at Laboratoire de Thermocinétique, Nantes (Bardon [36], Cassagne [37, 38])

2.3.2 Error analysis and model

2.3.2.1 Surface temperature measurement

The surface heat exchanges are modified by the presence of the sensor which does not have the same thermophysical and radiative properties and the same convective heat transfer as the medium to which it is applied. Therefore, a parasitic heat flow is transferred from the medium towards the sensor then from the sensor towards the environment as illustrated in figure 2.18. for surface temperature measurement.

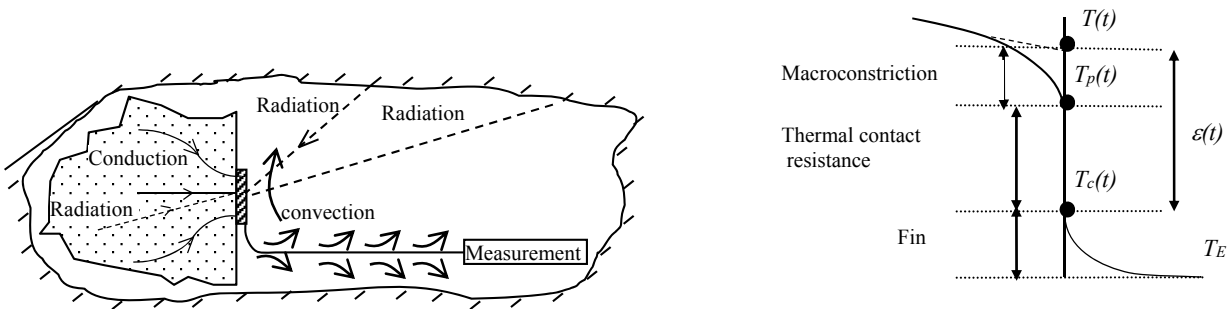


Figure 2.18.. Surface temperature measurement

A heat generation or absorption closed to the sensor or to its connection can also occur. All these transfers induce, at the measurement location, a local temperature disturbance which can be either positive or negative according to the heat direction (going in or out). The temperature is no more T but T_p . Moreover, the sensor temperature is not usually equal to T_p because the imperfect contact conditions between sensor and medium involves a temperature discrepancy $T_p - T_c$ which increases as the thermal contact resistance or the heat flux increases.

For an opaque medium, the following three effects are combined:

1. the effect of convergence of heat flux lines towards the sensor (macroconstriction effect),
2. the effect of thermal contact resistance which involves a temperature jump at the sensor/medium interface, and
3. the fin effect which corresponds to the heat transfer towards the outside (over the sensor and along its connection wires).

The measurement error is then:

$$\varepsilon(t) = T(t) - T_C(t)$$

2.3.2.2 Temperature measurement within a volume

For temperature measurement within a volume, the analysis is similar to the previous one. The error independently of the chosen sensor depends on the fact that the sensor temperature almost never coincides with that of the small element which it replaces. The thermophysical characteristics of the sensors (λ , ρ , c) and its radiative properties are different from those of the medium.

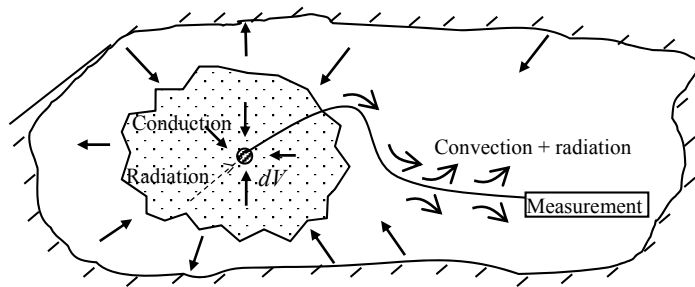


Figure 2.19. Temperature measurement within a volume

Heat transfer within the medium is modified by the presence of the sensor and similarly to surface temperature measurement, a local disturbance of the temperature field appears due to the heat transfer from the medium to the outside through the sensor. One still finds the three effects of: 1) convergence of the heat flux lines towards the sensor. 2) the thermal contact resistance effect 3) the fin effect. In addition the error is still : $\varepsilon(t) = T(t) - T_C(t)$

2.3.2.3 Error model

The study of the error related to the disturbance of the local temperature requires the solution of a multidimensional heat transfer problem with various possible configurations and boundary conditions. In this section, one will use relatively simple but very typical models that will clearly show the respective role of conduction within the medium, of non perfect contact between sensor and medium and finally the heat exchanges towards the environment. Most of the conclusions could be extended to numerous others configurations.

We will suppose that the heat exchanges of the medium or of the thermometric connection with the environment can be represented by the heat transfer coefficient, h , and the outside equivalent temperature, T_E . It is known, for example, that for a surface which absorbs a heat flow F (radiation coming from a high temperature heat source) which exchanges by convection with a fluid at T_f temperature and by radiation with walls at temperature T_0 , one have:

$$h = h_c + h_r$$

$$T_E = \frac{h_c T_f + h_r T_o + F}{h}$$

where h_c is the convection heat transfer coefficient, $h_r = 4A\sigma T_m^3$ the radiation coefficient (A is a coefficient which depends on the emissivity and of the relative location of surfaces between which the radiative heat exchange occurs, T_m is an intermediate temperature between T_o and that of the surface).

2.3.2.3.1 *Steady state surface temperature measurement of an opaque medium*

One will investigate surface temperature measurement on an opaque medium of thermal conductivity λ with a simplified sensor having the shape of a rod perpendicular to the surface (figure 2.20.). Far from the sensor, the medium is at the constant temperature T . The surface of the medium is assumed adiabatic except at the contact area S with the sensor.

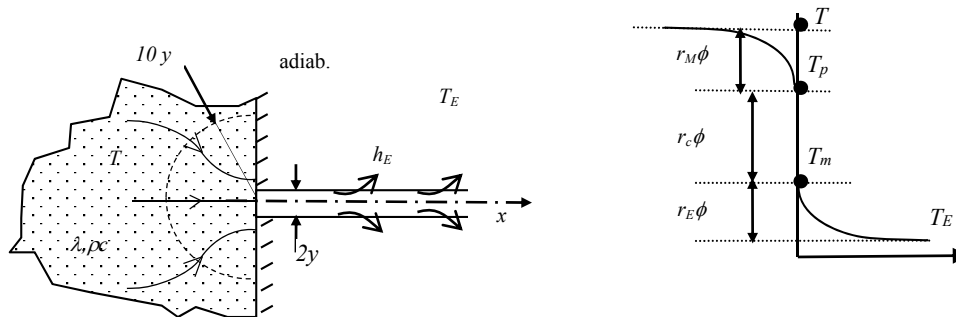


Figure 2.20. Steady state configuration

The three following effects occur due to heat leakage through the sensor towards the outside :

a) *The convergence effect* : it results from the relation between true temperature and disturbed temperature:

$$T - T_p = r_M \phi \quad (2.31)$$

where r_M is a macroconstriction resistance and ϕ the parasitic heat flux . With 3D heat transfer calculation, one can show that $r_M \cong \frac{0,4789}{\lambda \sqrt{S}}$ and for a circular surface of radius ρ : $r_M = \frac{l}{4\rho_o \lambda}$. It is also shown that 96% of the $T - T_p$ temperature drop is within an hemisphere of center 0 and radius 10ρ or $5,7\sqrt{S}$.

b) *The contact resistance effect* : responsible for the $T_p - T_c$ temperature drop, it is expressed by:

$$T_p - T_c = r_c \phi \quad (2.32)$$

where r_c represents the thermal contact resistance for the surface S (if R_c is the resistance per unit of surface: $r_c=R_c/S$). This effect is related to the imperfection of the contact which results from the irregularities of surfaces. The contact between two solid media is carried out only in some areas ($\sim 1\%$ of the apparent surface) between which remains an interstitial medium.

c) *The fin effect*: It is responsible for the heat transfer between the connection of the sensor and the environment. Whatever the assumed shape of the connection (rods with uniform or variable section)

the heat flux ϕ transferred from the face at $x = 0$ to the environment is linked to the temperature difference (between T_c at $x = 0$ and the equivalent outside temperature T_E) defined by:

$$T_c - T_E = R_E \phi \quad (2.33)$$

where T_c is the temperature at $x = 0$, T_E the equivalent outside temperature and R_E the total thermal resistance between the face $x = 0$ and the environment. It depends in particular on the geometry, the heat transfer coefficient and the thermal conductivity λ_E of this external connection :

$R_E = 1/(\pi y_E \sqrt{2h_E \lambda_E y_E})$ for a thermocouple assumed as a rod of radius y_E . From relations (2.31, 2.32 and 2.33), one can deduce the heat flux: $\phi = \frac{T - T_E}{r_M + r_c + r_E}$ and the measurement error :

$$\delta T = K (T - T_E) \quad (2.34)$$

$$\text{with } K = \frac{1}{1 + \frac{r_E}{r_c + r_M}} \quad (2.35)$$

The error is thus proportional to the measured and equivalent outside temperatures difference ($T - T_E$), the "error coefficient" K is all the more small as the sum of resistances of macro-constriction r_M and contact r_c will be small compared to the external resistance r_E . Therefore, it results that:

- For measurements on a high thermal conductivity medium (metal), $r_M \ll r_c$, the thermal contact conditions determines the errors
- For measurements on a low dielectric material, $r_M \gg r_c$, the effect of macroconstriction determines the error.
- The roles of r_E and T_E are finally very important. One needs the largest possible r_E and T_E nearest to T (probe with heat flux compensation). It is worth to focus one's attention to the heat flux ϕ_E generated on the surface of the connection wire. If T_E can becomes much higher than T , the error is changed by sign and is of great amplitude: it is necessary to avoid the external radiation of source on the connection. These conclusions, found for the temperature measurement on an opaque medium and for a simplified configuration of a sensor having the shape of a rod perpendicular to surface, remain valid with slight differences for real configurations.

2.3.1.3.2 Transient surface temperature measurement of an opaque medium

For a fast sudden contact between an opaque medium and a sensor assumed as a rod and perpendicular to its surface, the error becomes function of time: $\varepsilon(t) = K(t) [T(t) - T_E]$. It remains proportional to the temperature difference: $T(t) - T_E$

The coefficient $K(t)$ is maximum for $t \rightarrow 0$ and decreases for higher t values. For $t \rightarrow \infty$, one have: $K(T) \rightarrow K(\infty)$ which is obtained for a steady state. The contact conditions between sensor and medium are of great importance :

- If $r_c \neq 0$, $K(0) = 1$, the error is about 100% at $t = 0$ and decreases all the more the contact between sensor and medium is good.
- If $r_c = 0$ (perfect contact), the initial error is smaller:

$$K(0) = \frac{b}{b + b_E} < 1 \text{ where } b = \sqrt{\lambda \rho c} \text{ and } b_E = \sqrt{\lambda_E \rho_E c_E} \text{ are the medium and connection effusivities}$$

One can characterize the thermal inertia by the time response $x\%$, such as (figure 2.21.):

$$\frac{K(t_x) - K(\infty)}{K(0) - K(\infty)} = x$$

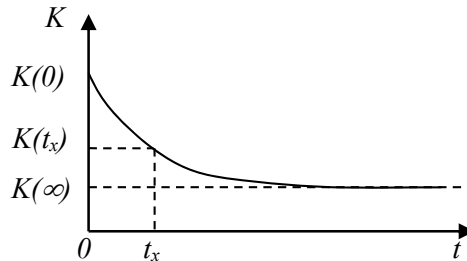


Figure 2.21.

For the same sensor t_x depends strongly on the characteristics of the medium and of the connection medium/sensor/environment. For a conducting medium, t_x depends strongly on r_c which appears as the main factor that determines the sensor inertia. t_x decreases when r_c decreases. It is the same thing if the diameter of the connections is reduced.

For fast transient evolutions, it is worth to weld wires on the surface, so that $r_c \rightarrow 0$, and to use wires as thin as possible. In this case ($r_c \sim 0$), the thermal inertia t_x is primarily determined by the establishment time t^* of the macro-constriction phenomena within the medium. In practice, this phenomenon remains extremely localized within the immediate vicinity of the sensor (hemisphere of radius $10y$), one can deduce an order of magnitude for t^* by considering the characteristic time $t^* \approx 100y^2/a$ associated to this hemisphere. %. One can consider that, at this time t^* , constriction is established at 97%. One can thus consider that $t_x \approx t^* \approx 100y^2/a$. For temperature with insulating mediums, r_c does not have any effect but t_x is much higher. For a transient evolution with a characteristic time t_c it is worth to choose a sensor for which $t_x \ll t_c$. In this case, as soon as $t > t_x$, the error will reach, at every moment, its minimal asymptotic value and the steady error model (K_∞) could be applied.

2.3.2.3.3. Temperature measurement within a volume

In this case, the connection wires usually do not follow an isothermal path on a sufficient length, therefore heat leakage through the sensors occurs. Measurements within a volume are in general much easier than on a surface and errors are usually smaller. However their analysis is more difficult to carry out especially because of the interaction between the connection wire and the medium. In addition, a cavity has to be realized for sensor introduction.

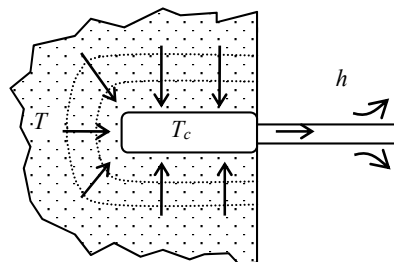


Figure 2.22. Temperature measurement with a cylindrical sensor inside the medium

Therefore, the cavity and sensors don't match exactly, so there exists, between them, some residual space filled with air, grease, glue... which introduces a thermal resistance between sensor and medium. The measurement errors introduced by these phenomena are qualitatively rather similar to those described for surface temperature measurements. Lastly, for long enough isothermal path, heat transfer between sensor and environment is negligible, the differences between thermophysical characteristics (conductivity, heat capacity) of the medium, of the probe or the wire of connection or residual space, introduce a localized disturbance of the thermal field, and a measurement error remains, but this one is much smaller. An example is provided in figure 2.22.

With this configuration the previous error model (2.34. and 2.35.) is still valid, the value of r_c and r_M being different. If we consider that the sensitive element of the sensor with a length L , and a radius y , which recovers its surface S , is isothermal and that its temperature is T_c (figure 2.22.). The contact between the probe and the medium is supposed to be imperfect, therefore for the whole surface of the sensor, the thermal contact resistance r_c is : $r_c = R_c/S$ with $S=2\pi yL$. If $T_E \neq T$, a heat flux occurs between the medium and the environment. The temperature field is modified. In this case the thermal constriction resistance is expressed by: $r_M = \frac{1}{2\pi\lambda\ell} \text{Log} \frac{2\ell}{y}$ if $\ell \gg y$

2.3.3. Practical consequence and examples, semi intrinsic thermocouples

2.3.3.1. Practical consequences

The steady state error model for the simple configuration allows some important features, most of them being valid for other configurations:

- 1) first of all even for perfect contact $r_c = 0$ there is an error which depends on the ratio r_M/r_E .
- 2) if the medium is a *high thermal conductivity* material, the macro-constriction r_M will be usually small relatively to r_c and the error will be especially determined by r_c . Thus, one must take care that r_c is small and remains stable. The contact pressure will have to be high and constant, surface will have to be plane without waviness, the interstitial medium with the highest possible thermal conductivity (welding, grease...). In addition, one should avoid oxide films as well as mechanical shocks and vibrations which can modify considerably r_c and consequently the measurement error.
- 3) For measurements on *an insulator*, r_M is large, usually much higher than r_c . Thus, the macro-convergence effect is the main factor in the measurement error and one can reduce it by increasing the radius of the sensitive element without increasing the section of the connections (figure 2.23.). A contact disc of high thermal conductivity material will be used.

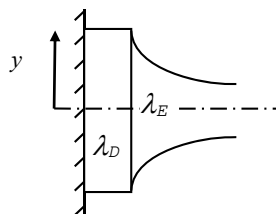


Figure 2.23.

- 4) Whatever the type of measurement, the fin resistance r_E should be as high as possible. The transversal area, the conductivity, the heat transfer coefficient have to be chosen the smallest possible. One also should have low emissivity surface, connection protected from high temperature fluids movements or radiation, T_E being modified in those situations. One should

note that having an insulating layer on the metallic wire of the thermocouple can increase the side heat transfer and therefore the measurement error.

- 5) Finally, the error is all the more small as T_E is close to the temperature to measure T . It changes with T_E . At the price of a technological complication, one can add an external heat source on the connection so that its temperature T_E is controlled in order to stay as close as possible as T . In this case, one reduces considerably the heat transfer and consequently the error of measurement. This principle is well known as “compensated heat flux sensors”. However for correct measurement, the thermal resistance r_E should stay high in order to prevent the compensation heating from disturbing the temperature field in the medium.

2.3.3.2. Application -for steady state temperature measurement for a thermocouple with and without a contact disc

The two thermocouple wires are considered as a unique rod with a radius $y_B = 0.5$ mm, an infinite length, an average thermal conductivity $\lambda_B = 15$ W.m⁻¹.K⁻¹ and a heat transfer coefficient $h_B = 5$ W.m⁻².K⁻¹.

The fin thermal resistance is : $r_B = \frac{l}{\pi y_B \sqrt{2 h_B y_B \lambda_B}}$ (rod approximation)

Thus, the connection resistance is:

- $r_E = r_B$ without contact disc,
- $r_E \approx r_B + \frac{l}{4 y_B \lambda_D}$ with contact disc

($\frac{l}{4 y_B \lambda_D}$ is the resistance due to heat flux convergence from y to y_B inside the sensor).

Table 2.9. provides the values of r_M , r_c , r_E and K and for various λ_D with and without disc ($y=y_B=10$ mm, $\lambda_D = \lambda_B$) and for different values of R_c per unit of area:

Table 2.9. Effect of medium thermal conductivity and of the disc on r_M , r_c , r_E and K

	Low thermal conductivity $\lambda=10^{-1}$ W.m ⁻¹ .K ⁻¹		High thermal conductivity $\lambda=100$ W.m ⁻¹ .K ⁻¹	
	without disc	with disc	without disc	with disc
r_M (K.W ⁻¹)	5000	250	5	0.25
R_c (K.W ⁻¹ m ²)	10 ⁻³	10 ⁻³	10 ⁻⁴	10 ⁻⁴
r_c (K.W ⁻¹)	1270	3,18	125	0,31
r_E (K.W ⁻¹)	1700	1733	1700	1733
K	0.786	0.127	0.072	0.0003

2.3.3.3. Temperature measurement with semi intrinsic thermocouple

In this device, one uses the medium M itself (presumably electrically conducting) as one item of the thermocouple (figure 2.24.). Compared to a traditional sensor, this device has several advantages:

- it has only one connection wire instead of two, thus heat leakage is reduced and the thermal resistance r_E is twice larger.
- the measured temperature T_μ is intermediate between T_p and T_c (figure 2.24.)

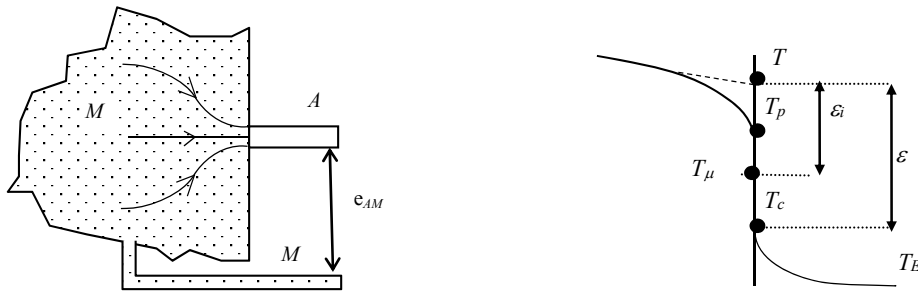


Figure 2.24. Semi intrinsic thermocouple

For times $t > t_c$ (time constant), T_μ is such that: $\frac{T_p - T_\mu}{T_\mu - T_c} = \frac{\lambda_A}{\lambda_M}$

The error $\epsilon_i = T - T_\mu$ is thus lower and the contact resistance effect is partly cancelled. For steady state, the error is such that:

$$\epsilon_i = K_i(T - T_E) \quad \text{with} \quad K_i = \frac{r_M + r_c \frac{\lambda_A}{\lambda_A + \lambda_M}}{r_M + r_c + r_E}$$

This error is considerably lower than with a traditional thermocouple (2 to 5 times) and this as much more as the wire thermal conductivity λ_A is small compared to λ_M . In transient mode, error and thermal inertia are greatly reduced (Bardon [36], Cassagne [37]). However, the calibration of the semi intrinsic thermocouple is almost always required. It is usually performed by comparison with a traditional thermocouple.

2.4. Heat flux measurement: direct and in direct methods

2.4.1. Direct measurement

2.4.1.1. Heat flux sensor with gradient (Ravaltera [39])

The principle of this heat flux measurement consists in directly applying the Fourier's law by measuring a temperature difference within the wall itself (intrinsic method) or by covering it with an additional wall (heat flux sensor-HFS-). The surface characteristics of this HFS should be close to those of the wall. The wall of the HFS can be homogeneous (the temperature difference is measured between its two main faces -normal gradient heat flux sensor- figure 2.25.-) or it can be heterogeneous creating heterogeneous temperature that is measured (tangential gradient heat flux sensor – figure 2.26.-).

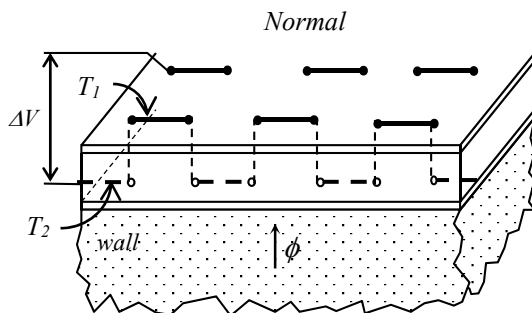


Figure 2.25.

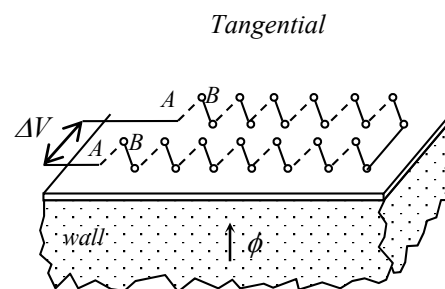


Figure 2.26.

The installation of such HFS on a wall, more or less disturbs the heat flux which crosses it. All must be done so that internal and contact thermal resistances are minimal. In these devices, the measurement of the temperature difference is performed using several thin film thermocouples or thermoresistances. These HFS can work whatever the heat flux direction in steady state or for slowly variable temperature.

2.4.1.2. Inertia heat flux sensor and heat flux sensor with electric dissipation (zero method)

Inertia heat flux sensors works only for variable temperature and if the heat flux is received by the wall. The HFS replaces a piece of the wall and is isolated from this one. Its surface characteristics are identical to those of the wall. The temperature increase of the HFS is proportional to the absorb heat flux and inversely proportional to its capacity (figure 2.27.). The choice of this one is very important because it determines the measurement sensitivity.

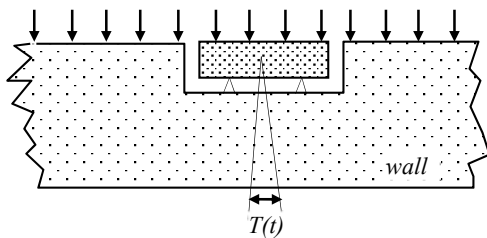


Figure 2.27.

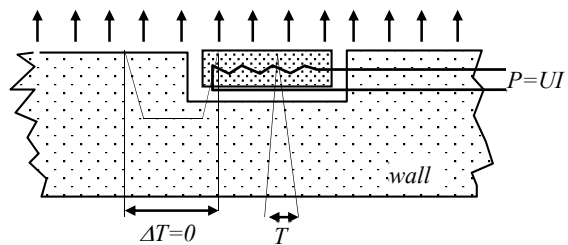


Figure 2.28.

The principle of this HFS with electric dissipation consists in substituting a piece of the wall at its surface with a small heating part insulated towards the wall (fig. 2.28.). The electric heating output is adjusted so that the surface temperature of the wall and of the heating part are equal ($\Delta T=0$). Thus, the dissipated electric flux is equal to the heat flux which leaves the wall in its immediate vicinity. This HFS works only for heat flux leaving the wall and for steady state or slowly variable temperature.

2.4.1.3. Enthalpic heat flux sensor

They are used to measure the heat flux coming from the outside. The HFS replaces an element of surface of the wall and is insulated from this one (figure 2.29.). An initially temperature controlled fluid circulation is heated by the heat flux which induces an enthalpic flow rate. For a correct measurement, the fluid temperature must be adjusted so that wall and HFS temperatures are almost equal. This condition is not always realized and can be an important source of error. The choice of the heat-storage capacity of the fluid also is important.

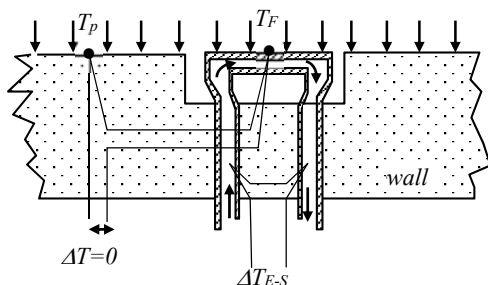


Figure 2.29.

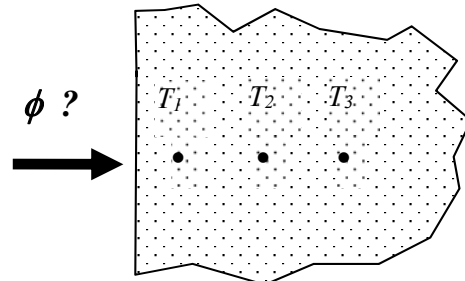


Figure 2.30.

2.4.2. Indirect measurement

One can obtain the surface characteristics (temperature T , heat flux φ) from measurements realized within the medium and using inverse methods (figure 2.30.). This procedure involves solution of ill-posed problems. Indeed, one cannot insure a solution, its uniqueness or stability. To solve such difficulties, the technique consists in replacing the ill posed problem by a well posed approximate problem. The solution is found by minimizing a norm of least square type. A heat transfer model (analytical or numerical) is required to solve the direct problem at each optimization step. These methods require significant developments (Beck [40], Alifanov [41], Ozisik [42], Jarny [43]). They will not be presented here. We will just underline that the solution of the inverse problem allows to compute the temperature residuals between final and measured temperatures. These residuals are of great importance because they allow to check the validity of the chosen heat transfer model. If no signature is observed (the residuals are purely random) the model is correct, otherwise the model should be improved.

With regard to the theoretical aspects of the instrumentation, Bourouga [44] has proposed criteria for correct locations of thermocouples to obtain unbiased results and also to optimize the experiment for wall heat flux or temperature estimation.

3. Thermal measurements using Scanning Thermal Microscopy (SThM)

This part of the lecture is strongly inspired of the Review Article "Scanning thermal microscopy: A review" to be published in the March 2015 issue of *Physica Status Solidi (a)* written by Gomès S., Assy A., Chapuis P. O.

Scanning Thermal Microscopy (SThM) techniques used miniaturized thermal probes and are based on Scanning Probe Microscopy (SPM) methods. Their spatial resolutions depend on the characteristic lengths associated to the heat transfer between the thermal probe and the sample to be characterized. Contrarily to far-field optical techniques, SThM is not limited in lateral resolution by optical diffraction at few hundreds of nanometres: it can perform thermal imaging and measurements far beyond the micron-scale. SThM probes can indeed be tailored with tips of curvature radii in the range of few tens of nanometres.

Because of its high spatial resolution, SThM is now an integral part of the experimental landscape in submicron heat transfer studies. Since the 1990s, it has been developed actively and applied to diverse areas such as microelectronics, optoelectronics, polymers, and carbon nanotubes.

3.1. Instrumentation and SThM methods

3.1.1. General principle

The first SPM instrument exploiting thermal phenomena for nanoscale measurements was invented in 1986 by Williams and Wickramasinghe [45], soon after the invention of Scanning Tunneling Microscopy. The goal was to extend the possibilities of imaging topography to insulators and was termed Scanning Thermal Profiler (STP). Although the STP was not intended for thermal imaging, it stimulated efforts to develop SPM-based techniques in the thermal area. Since then, various types of scanning thermal microscopes have emerged. These instruments have been mainly based on Atomic Force Microscopy (AFM), because AFM enables using a wider variety of samples and are very versatile systems. Measurements can be performed as a function of the tip-sample force and distance, and, as discussed in the following, various types of sensors can be placed at the tip of an AFM probe. Figure 2.31 describes the set-up of an AFM-based SThM system.

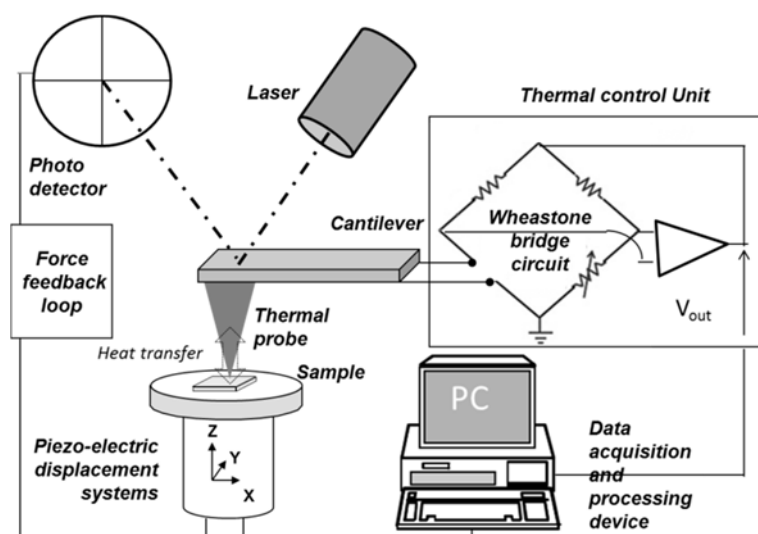


Figure 2.31. Set-up of an AFM-based SThM system. Here the output signal is the voltage V_{out} delivered by a “thermal control unit” and a balanced Wheatstone bridge can be used to maintain the probe mean temperature at constant value.

Cantilever deflections are probed by reflecting a laser beam on a reflective part of the probe, such as the cantilever itself or a mirror appropriately glued on its back, towards a photodiode. Other deflection measurement systems can involve piezoresistive cantilevers. The deflection generates an electrical signal that is detected. In the imaging mode, the deflection signal is used in a feedback control loop to maintain a constant tip-sample contact force while the tip scans laterally. Piezoelectric scanners are used to move the sample vertically and to scan the sample surface laterally. The combination of the X-Y scan position data, the force feedback signal and the thermal signal measured by the sensor located either at the tip or on the cantilever gives the raw data for both the topography image and the "thermal" image of the surface. The thermal image contrast reflects the change in the amount of heat locally exchanged between the tip and the sample. The force feedback control system operates simultaneously but, in contrast to the STP, independently of the process of the thermal measurement. Usually real-time thermal signal analysis is performed with the help of a thermal control unit.

Since 1993, various thermal methods based on the use of different thermosensitive sensors or phenomena have been developed. They can be classified according to the temperature-dependent mechanism that is used: thermovoltage, change in electrical resistance, fluorescence or thermal expansion. The lecture will mainly focus on thermovoltage-based and resistive methods.

3.1.2. Thermovoltage-based methods

Thermovoltage-based methods exploit the thermoelectric voltage generated at the junction between two electrodes to carry out thermometry (see *Section 2.1.2.*). Measurements can be performed either in the non-contact or contact modes in a STM or an AFM system.

Thermovoltage-based methods include the Tunneling Thermometry [46-49] and the point-contact thermocouple method [50] in which the thermoelectric junction is established between the tip and the sample surface (see *Section 2.3.3.3*). For both methods, thermal imaging with a nanometric spatial resolution was reported. However, the probe and the sample should have an electrically-conducting surface or a surface covered with a metallic film. This limits their applications.

Thermovoltage-based methods also involve probes with a built-in thermal sensor such as a thermocouple [51] and a Schottky diode [52]. The first is by far the most popular.

Advancements in microfabrication and characterization technologies have enabled to significantly improve the design, operation and use of thermocouple probes [51]. The miniaturization of the cantilever, the tip and the junction at the tip end could lead to a decrease of the probe thermal time constants and to an improvement of the spatial resolution. Figure 2.32 shows an example of nanojunction that it is possible to fabricate at the end of an AFM tip [53].

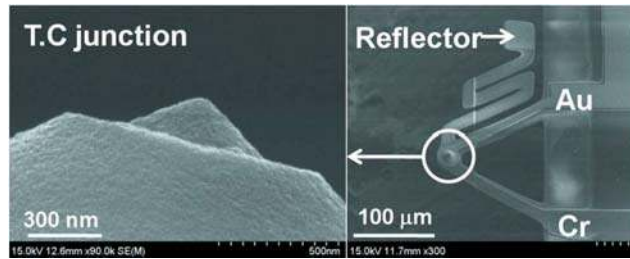
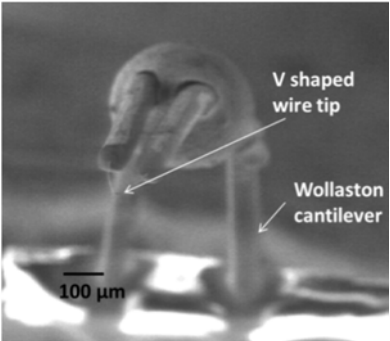


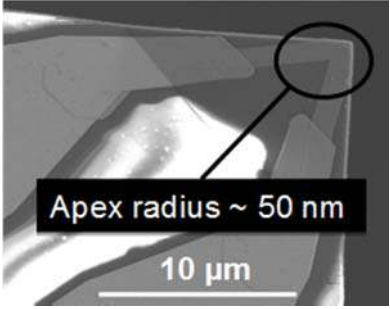
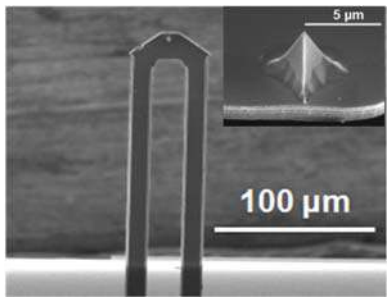
Figure 2.32. Scanning electron microscopy images of a Au–Cr thermocouple SThM probe. Reprinted with permission from [53] Copyright 2008, AIP Publishing LLC.

3.1.3. Resistive probes

Various kinds of SThM probes, based on resistance thermometry, in particular metallic probes and doped silicon probes, have been implemented. Table 2.10 gives the main characteristics of some examples of SThM probes currently used and commercialized.

Table 2.10. Characteristics of SThM probes currently used and commercialized

Main categories and Scanning electron microscopy image of resistive SThM probes	Description and main characteristics	Main applications
 <p>Figure 2.33. Wollaston wire probe [54].</p>	<p>Cantilever:</p> <ul style="list-style-type: none"> • Wollaston wire consisting of a silver shell of 75 μm in diameter and a core of an alloy of platinum and rhodium (Pt_{90%}/Rd_{10%}) of 5 μm in diameter [55]. • Spring constant of ~5 N/m. • Mirror stacked on the cantilever arms, so that the cantilever deflection can be controlled by optical way. <p>Thermosensitive element:</p> <ul style="list-style-type: none"> • at the extremity of the cantilever, • Wire of Pt90/Rd10 bent in a V-shape with a length of approximately 200 μm. • Temperature coefficient $\alpha = 0.00166 \text{ K}^{-1}$ • Time response ~ 200 μs in air [56, 54]. 	<ul style="list-style-type: none"> • Microsystem diagnostics [58-60] • Thermophysical characterization of various materials [61-62] • Investigation of the thermal interaction between the probe and samples [54, 63-65]. <p>However its large active area limits the thermal investigations at nanoscales.</p>

 <p>Figure 2.34. Palladium probe [66].</p>	<p>Cantilever [67]:</p> <ul style="list-style-type: none"> • Silicon oxide or silicon nitride. • Spring constant of ~ 0.35 N/m. • Tip height around $10 \mu\text{m}$. <p>Thermosensitive element [68]:</p> <ul style="list-style-type: none"> • Thin Pd film positioned at the very end of a flat tip located at the extremity of a thin cantilever. • Tip curvature radius of around 50 nm. • Temperature coefficient: $\alpha \sim 0.0012 \text{ K}^{-1}$. • Time response \sim a few tens of μs. 	<ul style="list-style-type: none"> • Thermophysical characterization of various materials [69-71] • Investigation of the thermal interaction between the probe and samples [66].
 <p>Figure 2.35. Doped Silicon probe (DS probes) [66].</p>	<p>U-shaped cantilever:</p> <ul style="list-style-type: none"> • two micrometric legs with high-doping level and a low-doped resistive element platform. <p>Tip:</p> <ul style="list-style-type: none"> • mounted on top of the resistive element. • of nanometric curvature radius (it can reach 10 nm), micrometric height and conical or pyramidal shape <p>Operating in active mode. Note that the first-order expansion of (2.36) is not sufficient to describe the variation of the electrical resistance as a function of temperature for this probe.</p>	<ul style="list-style-type: none"> • Nanothermal analysis, • Thermomechanical actuation, • Nanolithography, • Data storage. <p>A review of its applications is given in [72].</p>

All resistive metallic probes can also be used in passive and active modes.

The passive mode is used for thermometry. In this mode, a very small electrical current is passed through the probe. This results in minimal Joule self-heating and enables the measurement of the electrical resistance. During a scan, heat flows from the hot sample to the probe changes the electrical resistance R_p of the probe. Indeed at first order:

$$R_p(T) = R_{p0}(1 + \alpha(T - T_0)) \quad (2.36)$$

where $R_p(T)$ is the electrical resistance of the probe thermosensitive element at a reference temperature T , R_{p0} is the electrical resistance of the element at temperature T_0 and α is the temperature coefficient of its electrical resistivity.

The active mode is used to measure thermophysical properties of materials such as thermal conductivity. In this case, a larger electrical current is passed through the probe, resulting in a significant Joule heating. Part of the Joule power flows into the sample, depending on its thermal conductivity. The probe temperature is monitored by measuring the probe voltage. This temperature is related to the thermal conductivity of the sample.

The active mode can also be used to locally heat the sample in order to induce and study thermo-dependent phenomena such as in *Scanning Thermal Expansion Microscopy* or with the dynamic localized thermomechanical analysis method, both developed by Hammiche *et al.* in 2000 [61].

Under both passive and active modes, dc, ac or both measurements can be performed. Exciting the probe with an ac electrical current can be useful for an improved signal-to-noise ratio, since lock-in detection is possible. It is worth mentioning that a 3ω method can be used [56], which consists in measuring the third-harmonic voltage $V_{3\omega}$ of the resistor. The $V_{3\omega}$ amplitude is directly proportional to an increase of temperature due to Joule heating: $V_{3\omega} = \alpha T_{2\omega} \cdot R_{p0} I_{\omega} / 2$, where I_{ω} is the amplitude of the exciting current and $T_{2\omega}$ is the amplitude of second-harmonic of the probe mean temperature. Different configurations of electrical bridge can be used to measure the electrical resistance of the probe and deduce its temperature.

3.1.4. Other methods

In addition to the thermoresistive and the thermocouple phenomena, few other thermally-dependent physical effects can be exploited for thermal investigations at the micro and nanoscale:

- Thermoacoustic effect [73-75],
- Bimetallic probes [76],
- Fluorescent-particle based tips [77].

3.2. SThM measurement approaches

3.2.1 Energy balance

As in all thermal measurement method involving a sensor in contact or in proximity with the sample surface to be characterized, the quantity of heat exchanged between the sample and the tip Q_{s-t} depends on the energy balance of the system that consists of the sensor in contact with the sample and interacting with its surrounding environment (see Section 2.3.2 and Figure 2.36). Q_{s-t} is consequently a function of the effective thermal properties of sample and probe, and temperatures of probe, sample and their surrounding environment.

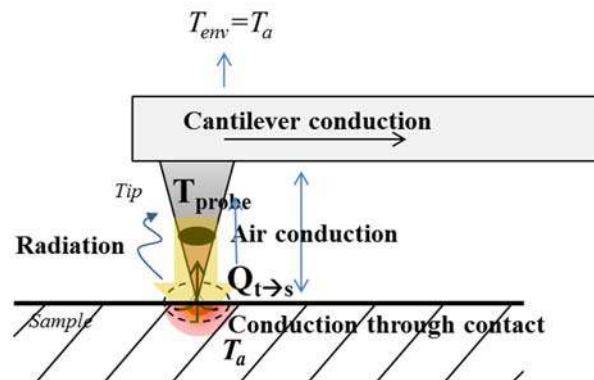


Figure 2.36. Schematic diagram of the heat flow within the system probe-sample-surrounding environment for a probe used in passive mode and in contact with a hot sample. Not at scale.

3.2.1.1. Thermometry in steady-state regime and passive mode

For thermometry in steady-state regime and passive mode, a heat quantity is exchanged between the hot sample and the probe that is initially at room temperature.

In a very simplistic way and as done in *Section 2.3.2.3*, this may be modelled by the thermal resistance network represented in Figure 2.37.

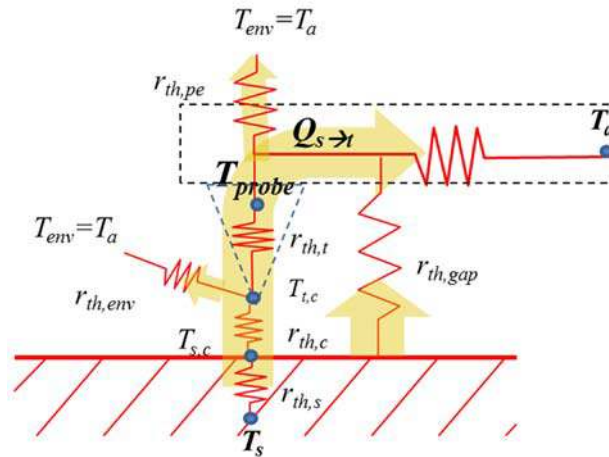


Figure 2.37. Thermal resistance network model for a probe used in passive mode.

Here T_{sp} is the sample surface temperature perturbed by the heat transfer between the sample and the cantilever far from the tip-sample thermal exchange area.

The corresponding expression of Q_{s-t} can then be written as:

$$Q_{s-t} = \frac{T_s - T_{t,c}}{(r_{th,s} + r_{th,c})} = \frac{(T_{probe} - T_a)(r_{th,pe} + r_{th,cant.})}{r_{th,pe} r_{th,cant.}} + \frac{T_{t,c} - T_a}{r_{th,env}} = \frac{(T_{probe} - T_a)}{r_{th,p}} \quad (2.37)$$

where:

- T_s is the sample temperature to be determined.
- T_{probe} is the probe temperature that is measured.
- The contact of the hot sample with the probe initially at ambient temperature T_a leads to a decreasing of the temperature within the sample under the probe-sample contact of temperature $T_{s,c}$ and an increasing of the temperature at the tip apex $T_{t,c}$.
- $r_{th,s}$, $r_{th,c}$ and $r_{th,t}$ are the thermal resistances associated respectively to the heat transfer within the sample at the level of the constriction near the contact (sample thermal spreading resistance), to the heat transfer from the sample to the tip and to the heat transfer between the tip apex and the thermosensitive element of temperature T_{probe} .
- The heat losses to the environment are included in three thermal resistances: $r_{th,env}$ that describes the heat losses to the surrounding environment between the probe apex and the sensitive element, $r_{th,pe}$ that represents the probe heat losses after the sensitive element by convection and radiation to the environment and $r_{th,cant.}$ that corresponds to the heat losses by conduction in the probe support or cantilever.

Let $r_{th,p}$ be the equivalent for the last two thermal resistances. We note that a parasitic heat transfer from the sample directly to the cantilever, here represented by $r_{th,gap}$, can take place, but this will be neglected in the following.

In the simple case of a sensitive element at the tip apex, which is the case for almost all the thermovoltage-based SThM probes ($T_{t,c} = T_{probe}$ and $r_{th,env} = r_{th,t} = 0$), and no heat transfer between the cantilever and the sample surface, Q_{s-t} may be written as:

$$Q_{s-t} = \frac{T_s - T_{probe}}{(r_{th,s} + r_{th,c})} = \frac{(T_{probe} - T_a)(r_{th,pe} + r_{th,cant.})}{r_{th,pe} r_{th,cant.}} \quad (2.38)$$

and the value of the correction to be applied to the nominal measurement of the instrument T_{probe} is:

$$\delta T = T_s - T_{probe} = \frac{(T_{probe} - T_a)(r_{th,s} + r_c)}{r_{th,p}} \quad (2.39)$$

This last expression shows that δT is dependent on the heat transfer within the sample (through $r_{th,s}$) and from the sample to the whole probe and its surrounding (through $r_{th,p}$). In addition, it depends on the heat transfer between the tip apex and the thermosensitive element if this last element is not located at the tip apex. δT also depends on the resistance of the tip-sample thermal contact r_c .

In practice, the error δT is very variable from a sensor to another one and from an experimental configuration to another one. The power rate transferred from the sample to the probe Q_{s-t} depends on many parameters characterizing:

- the surrounding gas (pressure, temperature, degree of relative humidity),
- the tip-sample mechanical contact: mechanical properties of tip and surface, tip-sample force, surface roughness and topography,
- the thermophysical properties of probe and sample.

As shown in the *Section 3.2.2*, experimental calibration methodologies have been proposed for the determination of δT . The estimation of all the involved parameters through modelling is not trivial and is still one of the main limitations of SThM involving nanoprobes. Indeed, heat transfers at micro and nanoscales within the tip and sample, exchanged between the probe and the sample through surrounding gas and radiation or through nanoscale contacts must be considered in the estimation of δT . The tip-sample heat transfer is described in details in *Section 3.4*.

3.2.1.2. Thermophysical measurement (active mode)

In this case, the heating of the sample by the probe operating in active mode (in dc or ac regimes) is required. The temperature sensor is heated through Joule effect and plays the role of heat source for the sample (Figure 2.38). Under this condition, the rate of the heat transferred by the probe to the sample Q_{t-s} may be written as a function of the thermal power P used for the heating of the probe, the measured probe temperature T_{probe} . (see in Figure 2.38):

$$Q_{t-s} = (T_{t,c} - T_a)/(R_{th,s} + R_{th,c}) = P - ((T_{t,c} - T_a)/R_{th,env} + (T_{probe} - T_a)/R_{th,p}) \quad (2.40)$$

$R_{th,p}$ includes here the possible thermal losses from the cantilever to the sample.

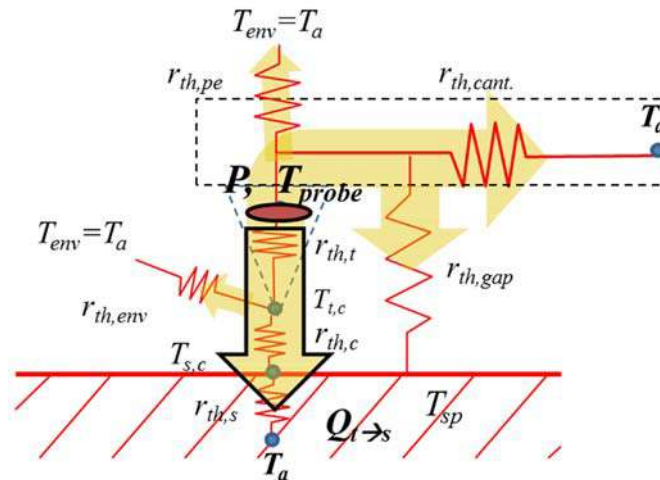


Figure 2.38. Thermal resistance network model for a probe used in active mode.

For bulk and homogeneous thick samples, the sample thermal conductivity k_s is included in the expression of the sample thermal spreading resistance $r_{th,s}$ that can be written as:

$$r_{th,s} = \frac{1}{4\lambda_s b} \quad (2.41)$$

if one assumes that the heated area on the sample surface is circular of effective radius b and isothermal [78].

From (2.40) and (2.41), the ideal situation for an easy estimation of the sample thermal conductivity should be that

- (i) λ_s is included in the expression of $r_{th,s}$ only and,
- (ii) the tip apex temperature $T_{t,c}$ equals the averaged probe temperature T_{probe} that is measured by the thermal sensor through the measurement of its electrical resistance in the case of a resistive probe.

However, as discussed by *Majumdar* in [51], even assuming the thermal resistance to the heat transfer from the sample to the tip $r_{th,c}$, b and $T_{probe} = T_{t,c}$ ($r_{th,t} = 0$) as constant whatever the sample is, Q_{t-s} :

$$Q_{t-s} = 4\lambda_s b (T_{t,c} - T_a) / (1 + 4\lambda_s b r_{th,c})$$

For Q_s to depend primarily on λ_s , $4b\lambda_s r_{th,c} \ll 1$ must be satisfied, that is, the dominant thermal resistance should be that of the sample.

As an example, in the case of the Wollaston probe (Figure 2.33) and experiments performed under ambient, the order of magnitude of $r_{th,c}$ and b have been estimated to be about $5 \cdot 10^6 \text{ K} \cdot \text{W}^{-1}$ to $8 \cdot 10^6 \text{ K} \cdot \text{W}^{-1}$ and several micrometers [66] respectively. Consequently, SThM measurements with this probe would mainly be sensitive to λ_s for materials of low thermal conductivity. It has been demonstrated that this is effectively the case [54, 56, 66].

Depending on the probe, various analytical and numerical models have been proposed to link the nominal signal effectively measured (voltage) and the parameters to be determined (λ_s).

For resistive probes, the thermal sensor cannot be assumed to be located at the probe apex. The probe temperature at the probe apex $T_{t,c}$ must be known to rigorously establish the expression of the heat rate exchanged between the probe and the sample. The most used analytical thermal model is based on the resolution of the conduction equation in the probe described as thermal fins [56, 79]. The model then considers geometrical and dimensional parameters and the physical properties of materials to describe the probe and include effective parameters such as:

- an effective coefficient h of heat losses by the whole probe surface to its environment, which is key to the expression of the thermal resistance $r_{th,pe}$ in figure (2.38).
- the effective thermal resistance $r_{th,c}$ generally used for describing the probe-sample thermal interaction at the level of the probe-sample contact. Thermal interaction is then assumed to take place across an area generally described as a disc of effective radius b at the sample surface.

Such model allows the determination of the mean temperature of the thermosensitive element of probe whatever the regime dc or ac of probe heating is.

As explained in the *Section 3.2.2.3.*, the comparison of such effective tip-sample system thermal model with measurements can also enable the determination of unknown modeling parameters such as $r_{th,c}$ and probe parameters such as the time response and the dimensional parameters of a sensor from measurements performed in ac regime.

Once calibrated for a given experimental configuration (probe and surrounding environment), the modelling is used to characterize unknown specimens from measurements performed in the same configuration.

3.2.2 Calibration

The calibration consists in performing measurements with a reference sample and comparing the determined value to the expected one. If they are not equal, one can correct the setting of the unit. In SThM, the calibration consists mainly in specifying the link between the thermovoltage (thermocouple junction) or the electrical resistance (resistive probe) measured with either the sample temperature or the sample thermal conductivity. Purely experimental methods with known samples and methods involving modelling of the measurement have been used.

3.2.2.1. Experimental calibration for thermometry

The calibration methods implemented for the determination of the error δT have mainly used laboratory self-heating samples. They have been based on comparisons of SThM measurements with either measurements obtained by optical thermometry methods or results of simulation of the sample surface temperature (or both). However optical thermometry methods have spatial resolution limited to few hundreds of nanometres and simulations at micro and nanometric scales are often dependent on simplifications or critical parameters. As a result, these comparisons are not always perfectly applicable to SThM temperature measurements with spatial resolution of few tens of nanometres, so precautions are necessary and limit the temperature measurement at nanoscales. One regularly evoked solution would be to exploit the null-point SThM (NP SThM method [81]) based on specific measurements which ensure that Q_{s-t} nullifies:

$$Q_{s-t} = \frac{T_s - T_{probe}}{(r_{th,s} + r_{th,c})} = 0 \quad (2.42)$$

Self-heating samples that have been used or fabricated for SThM calibration include instruments that are specifically designed for absolute temperature measurements on the scale of one micron. They are based on the measurement of the Johnson-Nyquist noise in a small metallic resistor [82], or instrumented membrane [83]. Other samples have been based on hot sources implemented in subsurface volume with a metallic line heated through Joule effect (see an example in [84]). The samples are generally heated in ac regime to demonstrate thermal mapping with low signal-to-noise ratio. They have been also used to characterize the dynamic response of sensors, which is also an important parameter to be considered.

Let us notice that accurate temperature measurements after calibration with such samples will only be possible on samples that hold surface properties close to the ones of the calibration samples.

3.2.2.2. Experimental calibration for thermal conductivity analysis

For thermal conductivity analysis, an experimental calibration can be performed with a set of experiments involving flat bulk samples of well-known thermal conductivities in a range that covers the expected value of the thermal conductivity λ_s to be measured (see an example of experimental calibration curve in Figure 2.39).

Let us consider the Wollaston probe (Figure 2.33). Practically, the tip is usually heated with an increase of temperature ΔT larger than 80 K to ensure a good signal-to-noise ratio and avoid issues related to the presence of a water meniscus [66, 85]. A stable dc current heats up the tip through Joule effect, and the electrical resistance of the tip is constantly monitored. The probe is measured with a balanced Wheatstone bridge that involves a feedback loop enabling to set a constant value of its electrical resistance, R_p . The average probe temperature $\overline{T_{probe}}$ is then kept constant during the measurement, and it is the electrical current I through the probe that can vary.

The data associated to each known sample are reported on a $\Delta P/P_{in}=f(\lambda_s)$ plot, where:

$$- P_{in} = R_p(\overline{T_{probe}})I_{in}^2$$

is the Joule power required to heat the tip at the set temperature when the tip is in contact with the sample of thermal conductivity λ_s , under this condition: $I = I_{in}$,

$$- \Delta P = P_{in} - P_{far} = (R_p(\overline{T_{probe}})I_{in}^2 - R_p(\overline{T_{probe}})I_{far}^2)$$

is the difference with the Joule power required to set the tip temperature when the probe is far from the contact [79].

Let us remark that the possible heating of the connecting wires due to internal Joule effect and thermoelectric effect at the contacts is here neglected.

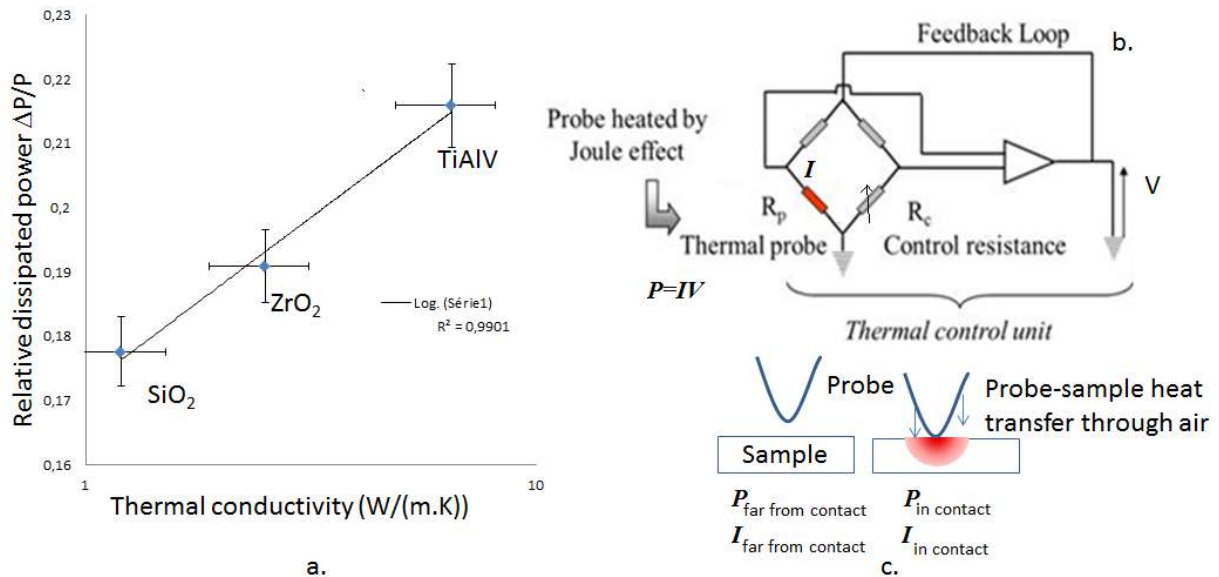


Figure 2.39. Experimental calibration curve. Three samples of known thermal conductivity in a range that covers the expected value of λ_s to be measured are used. b. Schematic diagram of a typical balanced Wheatstone bridge used for measurement with the Wollaston probe for investigating the thermal conductivity of samples. c. Principle of measurements with a probe free in air and in contact with the sample.

In principle, this experimental calibration is possible only for materials with comparable surface states (roughness, mechanical properties). Fortunately most of the heat is transferred through the air, not through the mechanical contact, when in ambient conditions. As a consequence, the experimental calibration is robust against probe and/or surface such as defects and irregularities in many cases. The method could furthermore be performed from measurements in ac. regime.

3.2.2.3. Calibration through comparison between measurement and modelling

As for numerous experimental methods of characterization, the fitting of simulated measurements with experimental data in well-known conditions can be used for the identification of the modelling parameters in SThM.

3.2.2.3.1 Probe parameters

The thermal resistance $r_{th,t}$, $r_{th,cant}$ and $r_{th,env}$, $r_{th,pe}$ depend on the shape and sizes of the probe.

For probes that have been partially made by hand, such as the Wollaston one, these parameters may vary from one tip to another. Even nanofabricated probes, which benefit from the reproducibility associated to cleanroom CMOS standard technology, may have little variations in the parameters. The user certainly does not want to inspect systematically all the tips with scanning electron microscopy (SEM). In addition, SEM check does not necessarily provide all the relevant information. For this reason, Lefèvre *et al.* [56] have proposed to use a sweep in frequency $V_{3\omega}(f)$ ($f = \omega/2\pi$ with ω the angular frequency) in order to determine the cut-off frequency f_c , which is linked to the size of the heating element in their Wollaston resistive tip (see figure 2.40).

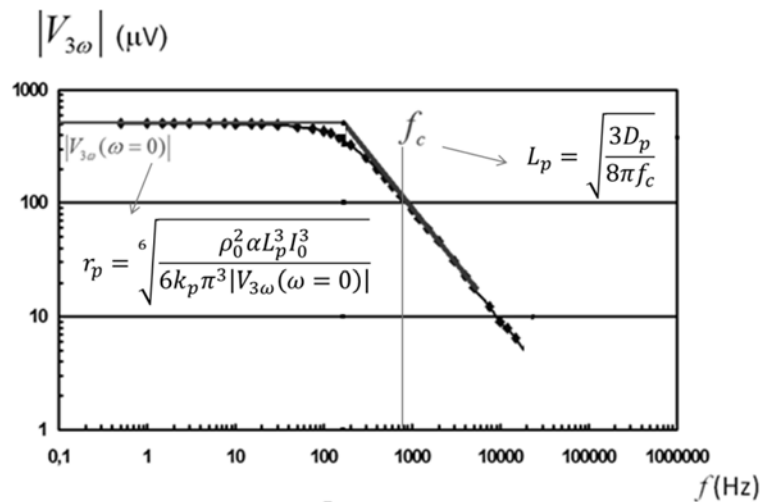


Figure 2.40. Modulus of the 3ω voltage $V_{3\omega}$ measured and simulated for a Wollaston probe as a function of the excitation frequency, $f = \omega/2\pi$, of the probe heating current. Fitting allows the determination of probe effective parameters.

The amplitude of the signal close to the static operation $V_{3\omega}(f \rightarrow 0)$ provides the radius of the filament, so that a full determination of the resistor is performed with such sweep. The method enables a useful direct experimental determination of some modelling parameters for the Wollaston probe.

Puyoo *et al.* [69] did similar analysis for the Pd probe and verified that its smallest dimension increases the value of the cut-off frequency, therefore higher-frequency operation and faster scans are possible.

The drawback of such characterization lies in the determination of f_c , with some uncertainty due to experimental measurement. These works used probes operating in active mode but such calibration can be performed for thermometry in a similar fashion [57].

3.2.2.3.2 Heat losses and probe-sample thermal interaction parameters

Modelling parameters, such as the effective coefficient h of heat losses by the whole probe surface to its environment and the effective parameters $r_{th,c}$ and b generally used for describing the probe-sample thermal interaction, can also be determined through the fitting of simulated measurement with experimental data in well-known conditions (various surrounding conditions, various frequencies of heating of the probe, various samples...).

The method has been used not only for thermal conductivity measurement of various materials [62, 66, 86] but also to study the probe-sample heat transfer. In particular, the comparison of a tip-sample heat transfer model with measurements under ambient air on a set of samples of various thermal conductivity has suggested that both $r_{th,c}$ and b depend on the thermal conductivity of sample [66]. Values of $r_{th,c}$ and b for the Wollaston probe were then respectively found varying from $5 \cdot 10^6$ K.W⁻¹ to $8 \cdot 10^6$ K.W⁻¹, and from few tens of μm to $1 \mu\text{m}$ when the sample thermal conductivity increases. Numerical simulation allowed to validate this values [66].

We note that an almost similar calibration methodology has recently been demonstrated comparing measurements performed with a Wollaston probe far from contact and without contact but at a small distance (< 100 nm) from the sample surface [86], confirming that heat transfer is mainly exchanged through air with the Wollaston probe [64, 66, 86] (see Section 3.3.4.).

It has also been demonstrated that this calibration methodology is applicable for the resistive palladium probe (figure 2.34) operated in air and under vacuum conditions [66].

Current Si probes with nanotips (figure 2.35) may be sensitive to a reduced range of thermal conductivities [87] compared to the one of larger and metallic probes. This is specifically due to nanoscale size effects. At room temperature the phonon averaged mean free path λ_{ph} in pure crystalline silicon is approximately 300 nm and exceeds the actual sizes of the tip apex of the Si probes. As a result a macroscopic description of heat transfer does not accurately model the heat flow and the heat conduction through the tip is modelled as quasi-ballistic transport. Mathiessen's rule can be applied to calculate a mean free path modified from the bulk value by accounting boundary scattering. Analytical expressions have already been proposed for simple geometries [88]. As a consequence an additional thermal resistance must be considered to describe heat transfer at the probe apex [89].

As discussed in the following, the expression of the sample thermal spreading resistance $r_{th,s}$ as well as the microscale description of the probe-sample heat transfer may also be strongly affected and fails due to nanoscale size effects.

Whatever the probe, a better understanding of the thermal interaction between a SThM tip and a sample is however crucial for a good understanding of measurement and a good interpretation of the contrast of thermal images. The following section focuses on the current description of the different heat transfers contributing to the probe-sample thermal interaction.

3.3. Probe-sample heat transfer

3.3.1. Heat transfer channels

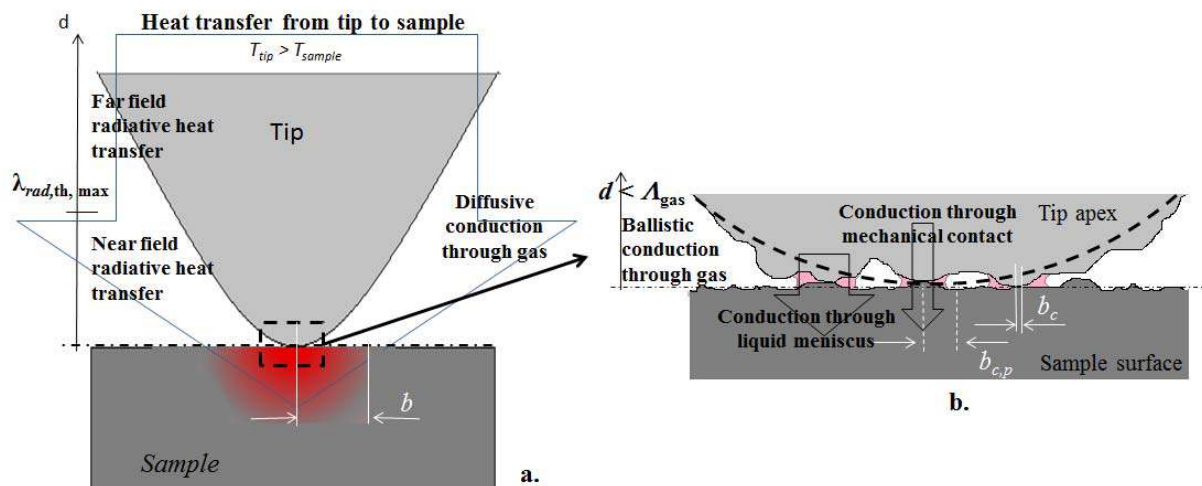


Figure 2.41. Schematic representations at different length scales (not at scale) of the heat flow paths from the very end of a heated tip at temperature T_{tip} to a sample at lower temperature T_{sample} .

- Microscopic probe-sample contact; b is the radius of the effective thermal contact.
- Microscopic multi-asperity contact. Dotted line represents the ideal profile of the tip apex. b_c and $b_{c,p}$ are respectively the mechanical contact radii associated to the ideal profile and the real profile of the tip apex.

Various mechanisms of heat transfer between the probe and the sample coexist. Figure 2.41 shows the heat flow paths from a hot probe to the sample for experiments performed under ambient air. The heat transfer channels between the probe and the sample include radiative heat transfer, thermal transfer through the surrounding gas, heat conduction through the liquid meniscus formed at the tip-sample junction and heat conduction through the mechanical contacts between both objects.

Very schematically, the effective thermal resistance $r_{th,c}$ describing the probe-sample thermal interaction at the level of the probe-sample interface may be written as (see figure 2.42):

$$r_{th,c} = \frac{1}{G_{th,c}} = \frac{1}{(G_{rad} + G_{gas} + G_w + G_{mc})} \quad (2.43)$$

with $G_{th,c}$ the effective thermal conductance describing the probe-sample thermal interaction, and G_{rad} , G_{gas} , G_w and G_{mc} , the thermal conductances describing the probe-sample heat transfer through radiation, gas conduction, liquid meniscus conduction and conduction through the mechanical contacts, respectively.

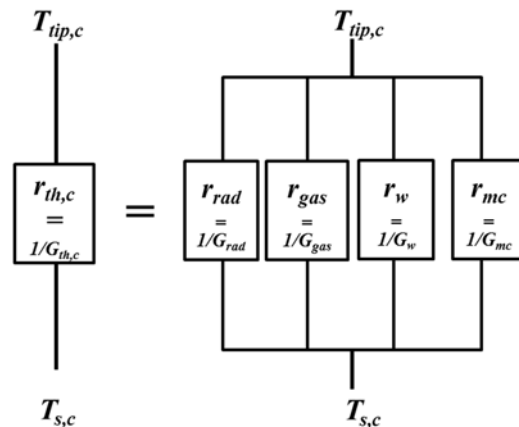


Figure 2.42. Thermal resistance network model of the thermal resistance of the probe-sample thermal interaction $r_{th,c}$: r_{rad} , r_{gas} , r_w and r_{mc} are respectively the thermal resistances describing the probe-sample heat transfer through radiation, gas conduction, liquid meniscus conduction and conduction through solids close to the mechanical contact. $T_{tip,c}$ is the mean temperature of the tip apex.

3.3.2. Thermal radiation

When not in vacuum, it is very difficult to determine experimentally the fraction of heat that is transferred or lost by thermal radiation. Very often, air heat transfer, by convection, diffusion or by ballistic heat transfer, cannot be distinguished from thermal radiation. As a consequence, it has been customary to neglect thermal radiation or to include it in the evaluation of another heat transfer mechanism [51, 90, 97]. This second way is particularly attractive when dealing with the air heat losses mentioned later, as thermal radiation toward environment can be embodied in the loss coefficient h .

However, it should be underlined that thermal radiation mechanisms are very different when the involved sizes are comparable to, or smaller than, the typical wavelength λ defined from Wien's displacement law $\lambda \cdot T = 2897 \mu\text{m} \cdot \text{K}$. Below few tens of micrometres (at room temperature), not only the classical thermal radiation mechanism (termed far-field) is possible, but also near-field radiative heat transfer due to tunnelling of evanescent surface waves generated by thermal motion [92-93]. This means that the transferred radiative heat flux can be increased by orders of magnitude in comparison to the far-field prediction [93]. This has been verified experimentally with bimetallic probes on which large

spheres were attached, to increase the area of exchange of thermal radiation [94]. It is also at the heart of the principle of the scanning thermal microscope developed by Kittel and colleagues, which is based on the non-contact heat exchange due to near-field heat transfer. The increase due to near-field is intense when the optical spectra of the material exchanging radiation are similar. When they are not, heat transfer is not as large and may not be very effective [94]. In addition, computation of near-field heat transfer may be dependent on the geometry while only few academic cases have been considered up to now. The impact of thermal radiation on SThM can be considered as an open question in many cases and should deserve intense research in the next years.

3.3.3. Air heat transfer

Heat can be transferred from the hot tip to the sample (or from the hot sample to the cold tip) through the air when the microscope is not located in vacuum. Indeed, a large area of the probe is in contact with the air lying around and can heat it. Hot air can then heat the sample.

It is important to note that the hot part of the tip can extend over tens of micrometres in some SThM probes. As a consequence, the heated part of the sample could potentially be as large, which raises questions about the spatial resolution of SThM. It has been shown that the heat flux deposited by the heated Wollaston probe, of micrometre size, can indeed extend over few microns [66]. As a consequence, this heat transfer mechanism is extremely efficient. 60% of the heat transferred from the Wollaston probe to the sample is carried by air at room temperature [95].

When the heater is far from the tip end and therefore from the sample (such as for the silicon tip), strong probe-sample air heat transfer also occurs, with air being heated at the area of the conical tip or directly by the cantilever.

When the tip-sample distance is large, heat convection can occur: the heat flux will be carried by the motion of air generated by the temperature difference [96].

At shorter distances (few micrometres and below), heat diffusion will be the main mechanism of heat transfer through the air. The heat transfer can then be modelled with standard Finite-Element Modelling (FEM) tools.

When the distance reaches few hundreds of nanometres, ballistic heat transfer will appear. The mean free path of the heat carriers, here air molecules (mostly nitrogen ones), λ_{air} becomes comparable with the tip-sample distance ($\lambda_{air} \sim 70$ nm at $P=1$ bar). In principle, FEM tools cannot be used anymore and more advanced methods have to be considered. However, if the area involved in ballistic heat transfer is much smaller than the one involved in diffusive heat transfer, the ballistic regime can be safely neglected. This may be the case in very-conical tips of micrometre sizes.

A large part of the heat can be lost in the air because heat lost by a hot tip does not necessarily flow towards the sample. For the Wollaston tip, this part of the Joule power is close to 40% [95]. It is therefore very important to precisely know the heat transfer coefficient h that describes the air-wall heat losses, in particular because its value can be different at micro or nanoscale than what is expected from macroscale correlations [95]. h can be identified by comparing the probe signal while working under ambient environment and under vacuum conditions where no transfer to the air is assumed. For the Wollaston tip, h is found around $3000 \text{ W.m}^{-2}.\text{K}^{-1}$ [98]. For the palladium probe, Puyoo [99] identified a value close to $6600 \text{ W.m}^{-2}.\text{K}^{-1}$. Kim and King [100] used numerical simulations and FE model to determine the heat losses to the air from the silicon cantilever of the silicon probes. The estimated

coefficient h around the leg was found about $2000 \text{ W}\cdot\text{m}^{-2}\cdot\text{K}^{-1}$ and around $7000 \text{ W}\cdot\text{m}^{-2}\cdot\text{K}^{-1}$ to the heater in the case of steady state heating.

All the values of h in the studies mentioned above show that heat losses are largely enhanced at small scale comparing to the values at the macroscale. We should mention that these studies identified the values of h when the probe is out of contact with the sample. Such values are susceptible to change when the probe comes to contact with the sample because of a restricted area of exchange between the probe and the environment medium. This effect has been neglected up to now.

3.3.4. Water meniscus

When the SThM probe contacts the sample, a water meniscus appears due to the capillary condensation of humidity. The heat path through water meniscus was scarcely studied in the literature and little information exists about the meniscus thermal conductance. The reason behind is that most of the properties of the water at small scales are still unknown and especially the thermal properties. Luo *et al.* [25] suggested in 1997 that the meniscus conductance G_w is dominant among the heat transfer mechanisms. Based on the Kelvin equation, G_w was given as:

$$G_w \approx 2\pi\lambda_w R_a \left[\ln \left(1 + \frac{R_a}{a} (1 - \cos\beta) \right) + 1 - \cos\beta \right] \quad (2.46)$$

Here, λ_w , a and R_a are respectively the meniscus thermal conductivity, the probe-sample separation and the apex radius, $\sin\beta = w/2R_a$ where $w=2r_2$ is the meniscus width as shown in figure 2.43.

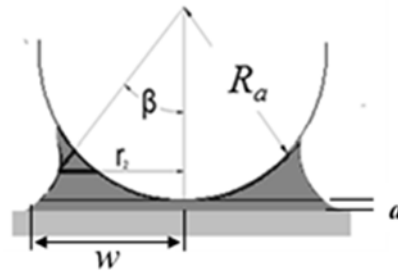


Figure 2.43. Schematic of the meniscus between the probe and the sample.

The probes of Luo *et al.* were made of thermocouple junctions (Au-Ni or Au-Pt) and the tip radius was around 100 nm. The thermal conductance determined from the experimental measurements was on the same order than the ones estimated using (2.46).

Using the same configuration of probe and sample, Shi *et al.* [101] later (in 2002) estimated that the heat transfer through meniscus is negligible in front of the heat transfer through air. The authors did not account for the thermal conductances at the probe-water and water-sample surfaces in their first work [25] and that was probably the reason behind such difference [101].

Taking into account these thermal conductances, Assy *et al.* [65, 66] have recently shown that conduction through water meniscus is not dominant in the probe-sample heat transfer interaction whatever the probe and its temperature (see figure 2.44). The values of the thermal conductances are lower one order of magnitude smaller than the values of the thermal conductance due to the heat transfer through air. The study was performed at various probe temperatures on samples of hydrophilic nature. The thermal conductance describing the heat transfer through the meniscus was estimated through the analysis of the capillary forces.

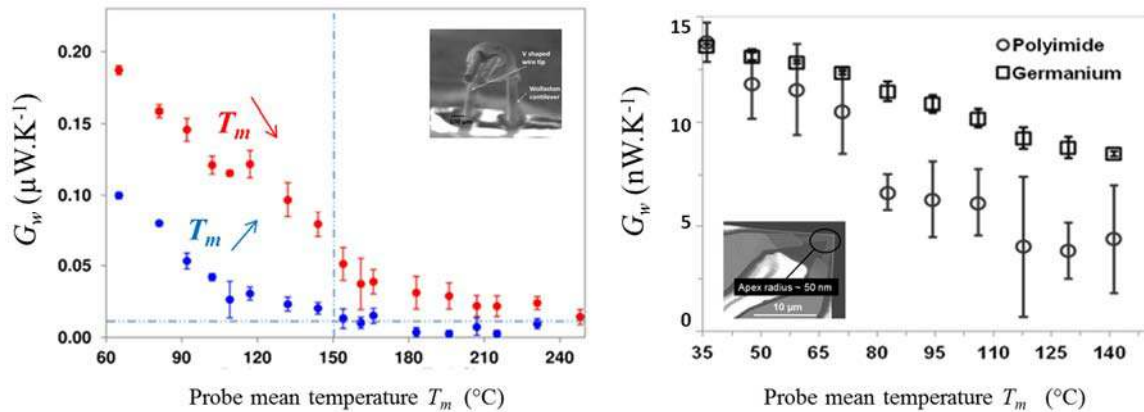


Figure 2.44. Variation of the total thermal conductance of water meniscus G_{total} as function of the probe mean temperature T_m for a contact between:
 (a) Wollaston probe and a sample of germanium (Ge) [65]
 (b) KNT probe and samples of polyimide and Ge [66].

Since the thermal conductance of the water meniscus depends on the dimensions of the meniscus, many factors might influence this heat path: hydrophilic or hydrophobic nature of the surfaces, roughness of surfaces, relative humidity.

3.3.5. Heat conduction at the tip-sample contact

The radius of the mechanical contact $b_{c,p}$ is generally estimated from mechanical contact theories such the ones developed by Hertz, Johnson–Kendall–Roberts (JKR) or Derjaguin–Müller–Toporov (DMT) for elastic deformation. These theories apply to the contact between a sphere and a flat surface and their use leads to consider an ideal contact between surfaces of perfect quality. Whatever the considered SThM tip, $b_{c,p}$ is estimated to be lower than a few tens of nanometres. For such nanoscale contacts, phonon mismatch and mechanical contact geometry have to be accounted for the estimation of the contribution of the solid-solid interface to the measurement.

An interfacial contact thermal resistance (thermal boundary resistance) should be considered at the tip-sample interface due to the difference in phonon dispersion between the two materials in contact [102-106]. This boundary resistance can be estimated as:

$$r_{th,contactB} = \frac{R_{th,B}}{\pi b_{c,p}^2} \quad (2.44)$$

with $R_{th,B}$ a thermal boundary resistance that has the same units as the bulk thermal contact resistance. Assy *et al.* [66] have recently shown that SThM measurement should allow the determination of $R_{th,B}$ for contacts with the probe material. The values that they obtained with the KNT probe corroborate the ones of $R_{th,B}$ experimentally determined for solid-solid contacts near room temperature (typically in the range $5 \cdot 10^{-7}$ to $5 \cdot 10^{-9}$ $\text{m}^2 \cdot \text{K} \cdot \text{W}^{-1}$).

Since the tip-sample interface is never perfect, (i) contamination or oxide layers can cover surfaces and (ii) the contact area is non-continuous due to surface roughness or weak coupling bonds between the atoms of solids.

Advanced contact models have been developed to account for the weak coupling. The transmission probability is then related to the mechanical coupling spring between the two solids [107-108].

Moreover, due to the roughness of the tip and sample surfaces, the apparent contact surface is not continuous. This surface can be divided into smaller contact area (of size b_c in Figure 2.41.b). Appropriate modelling of this effect depends on the ratio of the averaged mean free path of heat carriers Λ_c to the size b_c .

- If $b_c \gg \Lambda_c$, diffusive transport applies. Classical solutions are applicable:

$$G_{th,contact} = K\lambda_s b_c \quad (2.45)$$

where K is a geometrical factor describing the heat spreading within the sample (see (2.41)).

- If $b_c < \Lambda_c$, ballistic solutions must be considered [109].
- When $b_c \ll \Lambda_c$, the notion of finite contact spots may be extrapolated to the atomic scale [110-111].

Gotsmann [111] has recently suggested that a quantization of thermal conductance could occur when b_c becomes lower than λ_{coh} , the phonon coherence length, while the distance between individual contact spots may exceed λ_{coh} . This may take place e.g. for single-atom contacts. Related experimental works were performed under UHV with doped silicon probes with end tip specifically prepared for the purpose [111]. Under such environmental conditions, probe-sample thermal interaction involves near-field heat transfer and conduction through mechanical contact. From almost similar experiments under UHV, Pettes *et al.* [90] studied the phonon transport through a nanoscale point contact between a Si tip and a Si sample. Several models were used to evaluate the contact area critical for interpreting $r_{th,c}$. These works characterized the thermal boundary resistance $R_{th,B}$ for the considered Si-Si nanocontact by using a nanoconstriction model. These authors also examined the expression of the quantum thermal conductance and suggested the inaccuracy of such a model to explain measurement results obtained above room temperature [90].

Remarks:

The above discussion of roughness size effect may apply to the expression of the sample thermal resistance $R_{th,s}$ and its related effective radius b (see equation 2.41). $R_{th,s}$ dependence is strongly changed if $b \ll \Lambda_c$, and it no longer depends on the sample thermal conductivity. The contact becomes the essential parameter.

This seems to be an intrinsic limitation to SThM: the sensitivity to the thermal conductivity decreases as the characteristic size of the probed volume approaches the value of the averaged mean free path. If it becomes much smaller, the SThM measurement becomes completely independent of thermal conductivity. The measurement then provides directly information on the energy carrier properties [64].

Futhermore, if SThM should enable the investigation of thermal phenomena with a resolution sub-10 nm (it has already been the case in Tunneling thermovoltage-based SThM [46-49]), it is unlikely that temperature can vary within a distance of atomic spacing. Statistical thermodynamics states that temperature can be defined only when thermodynamic equilibrium is established.

4. Conclusion

Accurate temperature measurement is not an easy task. Errors depend on thermosensitive phenomena and also according to the sensors which can create local temperature disturbance and therefore bias.

Very often, this latter error is ignored. In this lecture dedicated to contact temperature measurement, one have tried to provide to the readers the know-how in various situations (temperature measurement in fluids or opaque medium) in order to perform the best temperature measurements as possible.

Thermal measurement at micro and nanoscales using Scanning Thermal Microscopy is furthermore presented. The crucial step of calibration and the limitations of the method are given. Finally, the complexity of the tip-sample heat transfer is discussed. This explains why its deep understanding is required in order to obtain the best achievements of the techniques.

5. References

- [1] Seebeck, T.J. 1823. Magnetische polarisation der metalle und erze durch temperatur-differenz, *Abh. K. Akad. Wiss.* Berlin, 265
- [2] Peltier, J. C. A. 1834. *Annales de Chimie et de Physique* 56: 371-470.
- [3] Thomson, W. 1848. On an Absolute Thermometric Scale founded on Carnot's Theory of the Motive Power of Heat, and calculated from Regnault's Observations, *Philosophical Magazine* 33:313-317.
- [4] Rathakrishnan, E. 2007. *Instrumentation, Measurements and Experiments in Fluids*, CRC Press.
- [5] Devin E. 1997. Couples thermoélectriques, données numériques d'emploi, *Techniques de l'Ingénieur*, tome R2594 :1-26.
- [6] Forney, L.J. and Meeks, E.L., Ma, J., Fralick, G.C. 1993. Measurement of frequency response in short thermocouple wires, *Rev. Sci. Instrum.* 64 (5) :1280-1286.
- [7] Yule, A.J. and Taylor, D.S., Chigier, N.A. 1978. On-line digital compensation and processing of thermocouples signals for temperature measurements in turbulent flames, *AIAA 16th Aerospace Sciences Meeting*, 78-80.
- [8] Lenz, W. and Günther, R. 1980. Measurement of fluctuating temperature in a free-jet diffusion flame, *Comb. and Flame* 37:63-70.
- [9] Lockwood, F.C. and Moneib, H.A. 1980. Fluctuating temperature measurements in a heated round free jet, *Comb. Sci. and Technology* 22:63-81.
- [10] Voisin, P. and Thiery, L., Brom, G. 1999. Exploration of the atmospheric lower layer thermal turbulences by means of microthermocouples, *E.P.J. App. Phys.* 7(2):177-187
- [11] Pitts, W.M. and Braun, E.B., Peacock, R.D., Mitler H.E. et al. 1998. Temperature uncertainties for bare-bead and aspirated thermocouple measurements in fire environnements, in Proceedings of the 14th Meeting of the United States Japan conference on Development of Natural Resources (UJNR) Panel on Fire Research and Safety, May, Japan.
- [12] Blevins, L.G. Pitts, W.M. 1999. Modeling of bare and aspirated thermocouples in compartment fires, *Fire Safety J.* 33(4):239-259.
- [13] Santoni, P-A. and Marcelli, T., Leoni, E. 2002. Measurement of fluctuating temperatures in a continuous flame spreading across a fuel bed using a double thermocouple probe. *Combustion and Flame* 131(1-2):47-58.
- [14] Rakopoulos, C. D. and Rakopoulos, D.C., Mavropoulos, G.C., Giakoumis, E.G. 2004. Experimental and theoretical study of the short term response temperature transients in the cylinder walls of a diesel engine at various operating conditions, *Appl. Therm. Eng.* 24(5-6):679-702.
- [15] Bardon, J.P. and Raynaud, M., Scudeller, Y. 1995. Mesures par contact des températures de surface, *Rev. Gén. Therm.* 34(HS95):15-35.
- [16] Paranthoen, L. and Lecordier, J.C. 1996. Mesures de température dans les écoulements turbulents, *Rev. Gén. Therm.* 35 :283-308.
- [17] Olivari, D. and M. Carbonaro. 1994. *Hot wire measurements. Measurements techniques in fluid dynamics. an introduction*, Von Karman Institut for Fluid Dynamics, *Annual Lecture Series*, vol. 1:183-218.

- [18] Million, F., Parenthoën, P., Trinite, M. 1978. Influence des échanges thermiques entre le capteur et ses supports sur la mesure des fluctuations de température dans un écoulement turbulent, *Int. J. Heat Mass Transfer* 21:1-6.
- [19] Bradley, D. and Mathews, K. 1968. Measurement of high gas temperature with fine wire thermocouple. *J. Mech. Engn. Sci.* 10(4):299-305.
- [20] Collis, D.C. and Williams, M.J. 1959. Two dimensional convection from heated wires at low Reynolds numbers. *J. of Fluid Mech.* 6:357-384.
- [21] Knudsen, J.G. and D.L. Katz. 1958. *Fluid dynamics and heat transfer*, Mc Graw-Hill Book Co., New-York.
- [22] Van der Hegg Zijnen, B.G. 1956. Modified correlation formulae for the heat transfer by natural and by forced convection from horizontal cylinders. *Appl. Sci. Res.* A(6):129-140.
- [23] Mac Adams, W.H. 1956. *Heat transmission*, Mc Graw-Hill Book Co., New-York.
- [24] Eckert, E. R. and Soehngen, E. 1952. Distribution of heat transfer coefficients around circular cylinders, Reynolds numbers from 20 to 500, *Trans. ASME, J. Heat Transfer*, 74:343-347.
- [25] Scadron, M.D. and Warshawski, I. 1952. Experimental determination of time constants and Nusselt numbers for bare-wire thermocouples in high velocity air streams and analytic approximation of conduction and radiation errors, NACA, T.N., 2599.
- [26] Tarnopolski, M. and Seginer, I. 1999. Leaf temperature error from heat conduction along the wires, *Agr. For. Meteo.*, 93(3):185-190.
- [27] Bailly, Y. 1998. Analyse expérimentale des champs acoustiques par méthodes optiques et microcapteurs de température et de pression, Ph. D. diss, University of Franche-Comté, France.
- [28] Fralick, G.C. and Forney, L.J. 1993. Frequency response of a supported thermocouple wire: effects of axial conduction, *Rev. Sci. Instrum.* 64(11):3236-3244.
- [29] Sbaibi, H. 1987. Modélisation et étude expérimentale de capteurs thermiques, Ph. D. diss, University of Rouen, France.
- [30] Singh, B.S. and Dybbs, A. 1976. Error in temperature measurements due to conduction along the sensor leads, *J. Heat Transfer* 491:491-495.
- [31] Kramers, H. 1946. Heat transfer from spheres to flowing media, *Physica* 12:61-80.
- [32] King, L.V. 1914. On the Convection of Heat from Small Cylinders in a Stream of Fluid, *Phil. Trans. of Roy. Soc. (London)*, Ser. A., 214(14):373-432.
- [33] Hilaire, C. and Filtopoulos, E., Trinite, M. 1991. Mesure de température dans les flammes turbulentes. Développement du traitement numérique du signal d'un couple thermoélectrique. *Rev. Gén. Therm.* 354/355 :367-374.
- [34] Castellini, P. and Rossi, G.L. 1996. Dynamic characterization of temperature sensors by laser excitation, *Rev. Sci. Instrum.* 67(7):2595-2601.
- [35] Hostache, G. and Prenel J.P., Porcar, R. 1986. Couples thermoélectriques à définition spatiotemporelle fine. Réalisation. Réponse impulsionnelle de microjonctions cylindriques. *Rev. Gén. Therm.* 299 :539-543.
- [36] Bardon J P 2001 « *Mesure de température et de flux de chaleur par des méthodes par contact*», Lecture c2b, Ecole d'Hiver METTI , Odeillo, 25-30 jan 1999, Vol.1, (Perpignan: Presse Univ).
- [37] Cassagne B, Bardon J P and Beck J V 1986 «*Theoretical and experimental analysis of two surface thermocouples*», Int. Heat Transfer Conf., San Fransisco.
- [38] Cassagne B, Kirsch G and Bardon JP 1980 *Int. J. Heat Transfer* **23** 1207-1217
- [39] Ravaltera G, Cornet M, Duthoit B and Thery P 1982 *Revue Phys. Appl.* **17** 4 177-185
- [40] Beck J V, Blackwell B and StClair C.A., 1985 *Inverse heat conduction* (New York: Wiley)
- [41] Alifanov O.M 1990 *Inverse heat transfer problems* (Springer)
- [42] Ozisik N 1993 *Heat conduction 2d ed.* (New York: Wiley)
- [43] Jarny Y, Ozisik M.N and Bardon JP 1991 *Int J Heat Mass Transfer* 34,11, 2911-2919
- [44] Bourouga B., Goizet V and Bardon J P 2000 *Int. J. Therm. Sci.* 39 96-109

- [45] Williams C. and H. Wickramasinghe, Scanning thermal profiler, *Applied Physics Letters*, 1986., 49(23), 1587-1589
- [46] Weaver J., Walpita L., and Wickramasinghe H., *Nature*, 1989. 342(6251): p. 783-785.
- [47] Nonnenmacher, M. and H. Wickramasinghe, *Applied Physics Letters*, 1992, 61(2), 168-170.
- [48] Zhou J., Yu C., Hao Q., Kim D. and Shi L., ASME 2002 International Mechanical Engineering Congress and Exposition, 2002.
- [49] Pavlov A., *Applied physics letters*, 2004, **85**, 2095-2097.
- [50] Sadat S., Tan A., Chua Y. J. and Reddy P., *Nano letters*, 2010, **10**, 2613-2617.
- [51] Majumdar, A., *Annual review of materials science*, 1999, 29(1), 505-585.

- [52] Leinhos T., Stopka M. and Oesterschulze E., *Applied Physics A: Materials Science & Processing*, 1998. 66, S65-S69.
- [53] Kim K., Chung J., Won J., Kwon O., Lee J. S., Park S. H and Choi Y. K., *Applied Physics Letters*, 2008, **93**, 203115.
- [54] Gomès, S., Ph.D Thesis, University of Reims, 1999.
- [55] Dinwiddie, R., R. Pylkki, and P. West, *Thermal conductivity*, 1993, **22**, 668-668.
- [56] Lefèvre S., Saulnier J.-B., Fuentes C. and Volz S., *Superlattices and Microstructures*, 2004, **35**, 283-288.
- [57] Ezzahri Y., Patiño Lopez L., Chapuis O., Dilhaire S., Grauby S., Claeys W. and Volz S., *Superlattices and Microstructures*, 2005, **38**, 69-75
- [58] Gomès S., Chapuis P.-O., Nepveu F., Trannoy N., S. Volz, Charlot B., Tessier G., Dilhaire S., Cretin B. and Vairac P., *IEEE Transactions on*, 2007. 30(3): p. 424-431.
- [59] Lopez L. D. P., Grauby S., Dilhaire S., Amine Salhi M., Claeys W., Lefèvre S., Volz S., *Microelectronics journal*, 2004, **35**, 797-803.
- [60] Altet J., Claeys W., Dilhaire S. and Rubio A., *Proceedings of the IEEE*, 2006, **94**, 1519-1533.
- [61] Pollock, H. and A. Hammiche, *Journal of Physics D: Applied Physics*, 2001. 34(9): p. R23.
- [62] Gomès S., David L., Lysenko V., Descamps A., Nychporuk T. and Raynaud M., *Journal of Physics D: Applied Physics*, 2007, **40**, 6677.
- [63] Lefèvre S., Volz S. and Chapuis P.-O., *International journal of heat and mass transfer*, 2006. 49(1), 251-258.
- [64] Chapuis P.-O., Ph.D Thesis, Ecole Centrale Paris, 2007.
- [65] Assy A., Lefèvre S. , Chapuis P.-O. and Gomès S., *Journal of Physics D: Applied Physics*, 2014. 47(44), 442001
- [66] Assy A., Ph.D Thesis, University of Lyon 2015.
- [67] Dobson P. S., Weaver J. M. and Mills G., *Sensors*, 2007 IEEE, 2007.
- [68] Puyoo E., Grauby S., Rampnoux J.-M., Rouvière E. and Dilhaire S., *Journal of Applied Physics*, 2011, **109**, 024302.
- [69] Puyoo E., Grauby S., Rampnoux J.-M., Rouvière E. and Dilhaire S., *Review of Scientific Instruments*, 2010, **81**, 073701.
- [70] Grauby S., Puyoo E., Rampnoux J.-M., Rouvière E. and Dilhaire S., *The Journal of Physical Chemistry C*, 2013, **117**, 9025-9034.
- [71] Saci A., Battaglia J.-L., Kusiak A., Fallica R. and Longo M., *Applied Physics Letters*, 2014, **104**, 263103.
- [72] King W. P., Bhatia B., Felts J. R., Kim H. J., Kwon B., Lee B., Somnath S. and Rosenberger M., *Annual Review of Heat Transfer*, 2013, **16**.
- [73] Majumdar A. and Varesi J., *Journal of Heat Transfer*, 1998. 120(2), 297-305.
- [74] Gurrum, S.P., et al., Scanning Joule Expansion Microscopy of a constriction in thin metallic film. *Journal of Heat Transfer-Transactions of the Asme*, 2005. 127(8): p. 809-809.

- [75] Deniset-Besseau A., Prater C. B., Virolle M.-J. and Dazzi A., *The Journal of Physical Chemistry Letters*, 2014. 5(4), 654-658.
- [76] Lai J., Perazzo T., Shi Z., Majumdar A., *Sensors and Actuators a-Physical*, 1997. 58(2): p. 113-119.
- [77] Saïdi E., Samson B., Aigouy L., Volz S., Löw P., Bergaud C. and Mortier M., *Nanotechnology*, 2009, **20**, 115703.
- [78] Yovanovich, M. and E. Marotta, *Thermal spreading and contact resistances. Heat Transfer Handbook*, 2003. 1: p. 261-394.
- [79] Lefevre S., Volz S., Saulnier J.-B., Fuentes C. and Trannoy N., *Review of scientific instruments*, 2003, **74**, 2418-2423.
- [80] David L., Gomès S. and Raynaud M., *Journal of Physics D: Applied Physics*, 2007, **40**, 4337.
- [81] Chung J., Kim K., Hwang G., Kwon O., Choi Y. K. and Lee J. S., *International Journal of Thermal Sciences*, 2012, **62**, 109-113.
- [82] Dobson, P., Mills G. and Weaver J., *Review of scientific Instruments*, 2005. 76(5), 054901
- [83] Thiery L., Toullier S., Teysieux D. and Briand D., *Journal of Heat Transfer*, 2008. 130(9), 091601.
- [84] Saïdi E., Babinet N., Lalouat L., Lesueur J., Aigouy L., Volz S., Labéguerie-Egée J. and Mortier M., *Small*, 2011, **7**, 259-264.

- [85] Gomès S., Trannoy N., and Grossel P., *Measurement Science and Technology*, 1999. 10(9), 805.

- [86] Zhang Y., Castillo E. E., Mehta R. J., Ramanath G. and Borca-Tasciuc T., *Review of Scientific Instruments*, 2011, **82**, 024902.
- [87] Nelson, B. and W. King, *Sensors and Actuators A; Physical*, 2007. 140(1), 51-59
- [88] Nelson, B.A. and W.P. King, *Nanoscale and Microscale Thermophysical Engineering*, 2008. 12(1), 98-115.
- [89] Gotsmann B., Lanz M. A., Knoll A. and Dürig U., *Nanotechnology*, 2010.
- [90] Pettes, M.T. and L. Shi, *Journal of Heat Transfer*, 2014. 136(3), 032401.
- [91] Joulain K, Mulet JP, Marquier F, Carminati R, Greffet JJ, *Surface Science Reports*, 2005. 57(3–4), 59-112.
- [92] Volokitin, A.I. and B.N.J. Persson, *Reviews of Modern Physics*, 2007. 79(4), 1291-1329.
- [93] Mulet JP, Joulain K, Carminati R, Greffet JJ, *Microscale Thermophysical Engineering* 6 (3), 209-222
- [94] Rousseau E., Siria A., Jourdan G., Volz S., Comin F., Chevrier J. and Greffet JJ., *Nat Photon*, 2009. 3(9), 514-517
- [95] Chapuis P.-O., Rousseau E., Assy A., Gomès S., Lefèvre S. and Volz S., *MRS Proceedings*, 2013, 1543, 159-164.
- [96] Lefevre, S., S. Volz, and P.O. Chapuis, *International Journal of Heat and Mass Transfer*, 2006. 49(1-2), 251-258.
- [97] Lefèvre, S., Ph.D Thesis, Université de Poitiers 2004
- [98] Chapuis, P.-O., JJ Greffet, K Joulain and S. Volz, *Nanotechnology*, 2006. 17(12), 2978.
- [99] Puyoo, E., Ph.D Thesis, University of Bordeaux 2010.
- [100] Kim, K.J. and W.P. King, *Applied Thermal Engineering*, 2009. 29(8), 1631-1641.
- [101] Shi, L. and A. Majumdar, *Journal of Heat Transfer*, 2002. 124(2), 329-337.
- [102] Prasher, R., *Nano letters*, 2005. 5(11): p. 2155-2159.
- [103] Kelkar, M., P.E. Phelan, and B. Gu, *International journal of heat and mass transfer*, 1997. 40(11), 2637-2645.

- [104] Cahill D. G., Ford W. K., Goodson K. E., Mahan G. D., Majumdar A., Maris H. J., Merlin R. and Phillpot S. R., *Journal of Applied Physics*, 2003, **93**, 793-818.
- [105] Stoner, R. and H. Maris, *Physical Review B*, 1993. 48(22), 16373.
- [106] Swartz, E.T. and R.O. Pohl, *Reviews of Modern Physics*, 1989. 61(3), 605.
- [107] Prasher, R., *Applied Physics Letters*, 2009. 94(4), 041905-041905-3.
- [108] Persson, B., A. Volokitin, and H. Ueba, *Journal of Physics: Condensed Matter*, 2011. 23(4), 045009.
- [109] Prasher, R.S. and P.E. Phelan, *Journal of applied physics*, 2006. 100(6), 063538.
- [110] Mo, Y., K.T. Turner, and I. Szlufarska, *Nature*, 2009. 457(7233), 1116-1119.
- [111] Gotsmann, B. and M. Lantz, *Nature materials*, 2013. 12(1), 59-65.